CHAPTER 1

BASICS OF ELECTRICAL MACHINES DESIGN AND MANUFACTURING TOLERANCES

1.1 INTRODUCTION

Recent progress in the area of electric machines, including new materials, manufacturing technologies, and conceptual topologies, require a systematic design approach to ensure improved performance and/or reduced cost for new developments. This chapter discusses fundamental aspects of the state-of-the-art design process and includes examples from industrial practice and case studies in order to introduce basic concepts and methods.

Traditionally, the core of electric machines is manufactured by punching and stacking thin laminations of cold rolled or silicon steel, as illustrated in Figure 1.1 [1]. Even with the rotor laminations nested inside the stator ones, the process results in a relatively large amount of steel being scraped due to the slots and outer stator profile. Depending on the machine type and design topology, in the rotor, permanent magnets (PM) maybe inserted or attached to the core, an electrically conductive cage maybe die-cast from aluminum, for example, or a winding (not applicable for the design shown in Figure 1.1) maybe inserted. The stator typically incorporates a collection of coils made of conductive wires separated by electrical insulation and forming a winding. A multiphase distributed winding, such as the one exemplified in Figure 1.1, maybe manufactured by automatically producing the coils and then inserting them into the core, in a process that has high through output, and results in a relatively high ratio of net conductor per slot area, that is, slot fill factor, but also yields relatively large end coils.

In order to reduce the scrap of laminated steel, different punching arrangements may be employed. The example shown in Figure 1.2 is particularly advantageous for stator designs with relatively large tooth width and small tooth tips. Modules of core and concentrated coils, each wound around a tooth, can be organized with a single or multiple teeth, formed to shape, and then assembled to produce a stator, such as

Multiphysics Simulation by Design for Electrical Machines, Power Electronics, and Drives, First Edition.
Marius Rosu, Ping Zhou, Dingsheng Lin, Dan Ionel, Mircea Popescu, Frede Blaabjerg, Vandana Rallabandi, and David Staton.

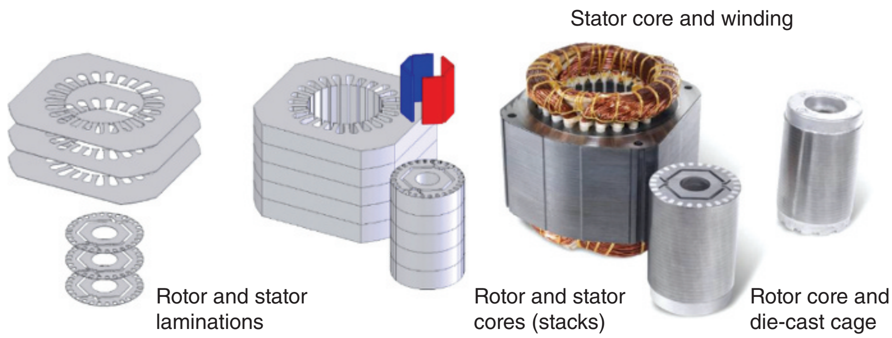

Figure 1.1 Typical steps for the manufacturing of an electric machine, in this case a line-fed permanent magnet (PM) synchronous motor, which includes in the rotor a die-cast aluminum cage.

the three-phase 18-slot design example from Figure 1.2, which is suitable to be used together with a 16-pole PM rotor [2, 3].

At a first look, concentrated windings, especially in a segmented-modular configuration, tightly packed with a high slot fill factor and short end coils maybe superior to more conventional distributed winding machines, particularly for low-speed applications. Nevertheless, before drawing such generic conclusions, systematic comparisons taking into account the power and speed rating, losses, including winding and core components, the electronic controller should be performed following, for example, a large scale automated design process as described in another chapter of the book.

A stator core and winding, and a rotor incorporating a shaft, are assembled together with other components, including bearings, end caps, and frame and terminal box to produce an electric machine, as exemplified in Figure 1.3 for a general-purpose three-phase squirrel-cage induction motor and in Figure 1.4 for PM

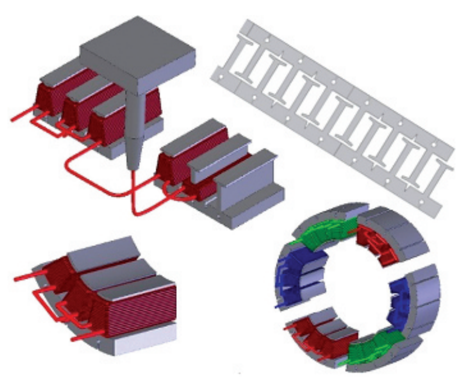

Figure 1.2 Example of stator modular construction with segmented core and concentrated coils forming a multiphase winding [2, 3]. Versions with a single tooth and coil modules are also possible.

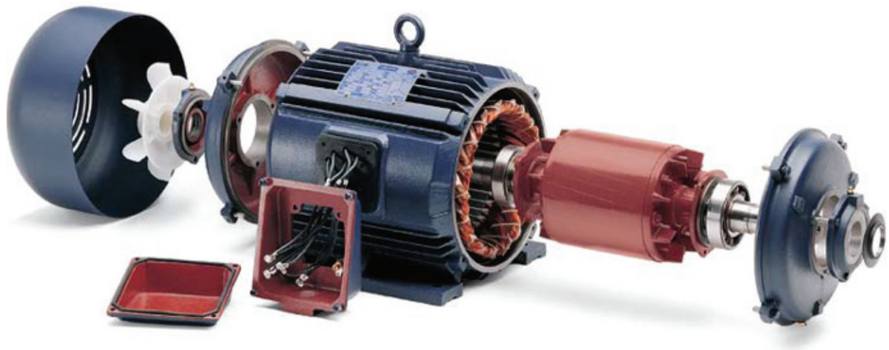

Figure 1.3 Exploded view of a general-purpose National Electrical Manufacturers Association (NEMA) frame squirrel-cage induction motor. *Courtesy of Regal Beloit Corp.*

synchronous motors with stator concentrated and distributed windings, respectively [4]. It should be noted that the use of PM technology typically results in a higher power density than available from induction machines.

A most successful example of combining advanced design techniques, high performance magnetic materials, and enhanced cooling is represented by the recent development of a 100 hp motor for Formula E racing cars [5,6]. This machine shown in Figure 1.5, which employs an 18-slot 16-pole spoke IPM configuration, sets a record for electric traction motors of comparable rating, achieving almost twice the specific torque density per unit of active mass (Nm/kg) than the motor powering the latest generation of the Nissan Leaf electric vehicle.

1.2 GENERIC DESIGN FLOW

In the overall economy of the electric machine design process, virtual prototyping is the most important collection of designing stages when considering design validation

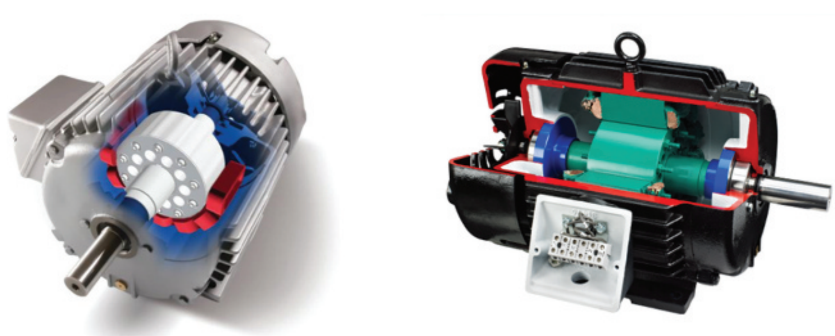

Figure 1.4 PM synchronous motors with interior permanent magnet (IPM) rotors and concentrated (left) and distributed windings, respectively [4]. *Courtesy of Regal Beloit Corp.*

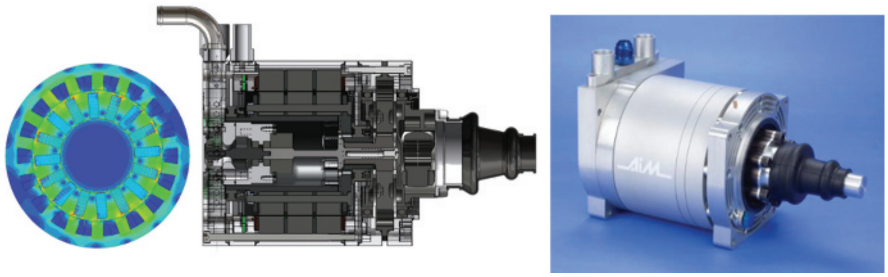

Figure 1.5 Record-breaking ultra-high density torque 100 hp spoke-type IPM motor for Formula E racing cars showing, from the left, magnetic field in the motor cross section, axial cut view and photo [4, 5]. *Courtesy of Equipmake, Ltd.*

before committing to making a physical prototype. The obvious procedures utilized throughout this process combine efficient numerical techniques providing with highly accurate, comprehensive multiphysics simulation designs including power electronics and control software to predict the electric drive performance at the heart of entire system.

The electrical machines are part of the electromechanical energy converters group. This means that any electrical machine, be it rotating, or linear movement, with AC or DC supply current, can operate as:

- Motor: conversion of the input electrical energy into output mechanical energy
- Generator: conversion of the input mechanical energy into output electrical energy
- Brake: absorption of both mechanical and electrical energy

In electromechanical terms, the main inputs and outputs of the electrical machines are the supply voltage and current versus the torque (or force) at the shaft and rotational (or linear) velocity.

The main design flow is shown in Figure 1.6. The initial design is addressed at the level of sizing stage when physical dimensions are established based on magnetic and thermal feedback. This is a specialized stage that allows designers to quickly create a geometric model of the machine, calculate its performance, and make sizing decisions. Once the initial design is completed, detailed numerical techniques (2D and 3D) are necessary to increase the accuracy of such designs by simulation. Such simulations are referred as physics-based designs whether the numerical technique relates to the electromagnetics simulation by finite elements or fluid dynamics solution by finite volumes or structural simulation by finite element analyses.

In this chapter, we will focus on the basic steps in designing a typical electrical machine for power traction application.

1.3 BASIC DESIGN AND HOW TO START

We will consider the specifications shown in Table 1.1 for a power traction application. If someone will ask what parameter would be the most important to determine

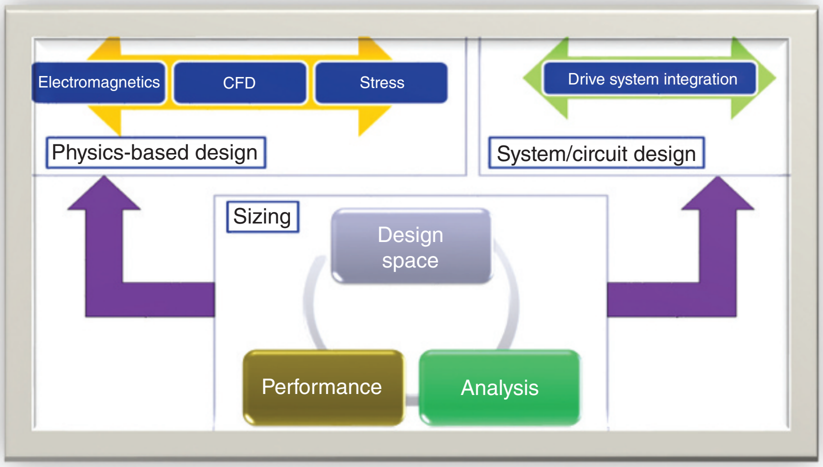

Figure 1.6 Multiphysics and multidomain electric machine design flow.

the physical dimensions of an electrical machine, we can definitely answer that the electromagnetic toque capability, which can be extracted from the design specification related to a certain application, will generate enough information to produce an initial magnetic design. And yet this is probably at the same time the most exquisite and intrigued statement one could deliver on such a complex design demand [7, 8].

Simply, following this rationale, the output torque is proportional to rotor volume and tangential force acting on rotor surface known as shear stress. The shear stress is proportional to the product of electric and magnetic loading. Besides electromagnetic torque, the rotor aspect ratio, stator slot diameter ratio, number of poles, and rotational speed are important parameters for design decisions.

TABLE 1.1 Power traction application specifications

Parameter	Unit	Value
DC supply voltage	V	400
Maximum DC current	A	700
Maximum line AC current	Arms	900
Peak output power	kW	235
Peak torque	Nm	330
Base speed	rpm	7500
Maximum speed	rpm	15,000
Continuous power at base speed	kW	80
Continuous torque at base speed	Nm	100
Cooling system	N/A	Liquid
System envelope volume	mm	270 × 270 × 270

The fundamental relationship for torque prediction is the equation which defines the force F acting on a wire of length L carrying a current I in a uniform magnetic field B as

$$F = B \cdot I \cdot L \tag{1.1}$$

If we consider a uniformly distributed conductor per meter, then we can introduce the shear stress as the ratio between force and area of conductive region. Thus,

$$\sigma = \frac{F}{\text{Area}} = B \cdot A \tag{1.2}$$

where B is also known as magnetic loading and A is known as electric loading.

In any electric machine with radial field concept with the rotor diameter D, the torque is introduced by

$$T = F \cdot \frac{D}{2} \tag{1.3}$$

In more general terms, the main parameter defining an electrical machine is the torque or force depending on the device that has a rotational or linear movement, respectively. In this design example, we are dealing with a rotational movement, for which the expression that provides the sizing **electromagnetic torque** is given by

$$T = \frac{\pi^2}{4\sqrt{2}} \cdot k_{w_1} A B D^2 L_{stk} \tag{1.4}$$

where k_{w_1} is the fundamental winding factor, L_{stk} is the axial active length.

A is the **electric loading**: number of ampere-conductors per meter around the stator surface that faces the airgap.

$$A = \frac{\text{Total ampere–Conductors}}{\text{Airgap circumference}} = \frac{2mN_{ph}I_{\text{RMS}}}{\pi D} \tag{1.5}$$

where N_{ph} represents the total number of turns/phase, I_{RMS} is the RMS phase current and m is the system number of phases.

B is the **magnetic loading:** average flux-density over the rotor surface. If the flux-density is distributed sinusoidal, the fundamental magnetic flux/pole (there are $2p$ magnetic poles in the electrical machine) is

$$\phi = B \cdot \frac{\pi D L_{stk}}{2p} \tag{1.6}$$

We notice from (1.4)–(1.6) that the torque, electric, and magnetic loading depend on the machine volume in the airgap.

Considering also the lossless **energy conversion** law for an m-phase AC machine,

$$\text{Electric power} = mEI = \text{Mechanical power} = T \cdot \frac{\omega}{p} \tag{1.7}$$

where E is the **induced voltage** (back electromotive force—emf), ω angular velocity. The induced voltage can be further developed as

$$E = \frac{\pi^2}{\sqrt{2}} \cdot \frac{f k_{w_1} N_{ph} B D L_{stk}}{p}, \tag{1.8}$$

where f is the fundamental frequency.

It is also worth noting the relation between fundamental frequency, f, number of pole pairs, p, and rotational speed n, where rotational speed is represented in revolution-per-minute (rpm),

$$f = \frac{n \cdot p}{60} \tag{1.9}$$

In sizing an electrical machine, we can use a combined parameter, that is, the torque ratio per volume based on relation (1.4) and knowing the rotor volume, $V_{\text{rotor}} = \frac{\pi D^2 L_{stk}}{4}$, then

$$TRV = \frac{T}{V_{\text{rotor}}} = \frac{\pi}{\sqrt{2}} \cdot k_{w_1} A \cdot B \tag{1.10}$$

The above equation reflects the electromechanical nature of the energy conversion, as A is proportional to the current in the machine windings, while B is proportional to the magnetic flux. Hence, the electric energy that is proportional to the product of magnetic flux ϕ and current I is converted to mechanical energy and relates to the torque production.

Table 1.2 summarizes the typical values for torque ratio per volume in various electrical machine types.

Another simple initial consideration is related to the current density in the electrical machine, depending on the cooling system (as represented in Table 1.3).

For the considered specifications, (as shown in Table 1.1) and assuming a split ratio (i.e., rotor/stator outer diameters) of 0.55, and that the active length of the machine occupies maximum 80% of the overall maximum axial length, we can estimate peak TRV as:

$$TRV_{\text{peak}} = \frac{330}{\frac{\pi \cdot (0.55 \cdot 0.27)^2 \cdot 0.27 \cdot 0.8}{4}} \cdot 0.001 = 88.20\ \text{kN/m}^3$$

TABLE 1.2 Typical values for TRV continuous operation in electrical machines

Electrical machine type	TRV (kNm/m^3)
Totally enclosed motors—low energy magnets (ferrite)	5–15
Totally enclosed motors—sintered rare-earth magnets (NdFeB, SmCo)	15–40
Totally enclosed motors—bonded rare-earth magnets (NdFeB, SmCo)	10–20
Medium power (>5 kW) industrial induction motors	5–30
Servomotors	15–50
Aerospace machines	30–75
Liquid cooled machines	75–250

TABLE 1.3 Typical current density values in electrical machines—continuous operation

Cooling system	Current density (A/mm^2)	Current density (A/in^2)
Totally enclosed non-ventilated	1–5	650–3250
Open air, fan cooled	5–10	3250–6500
Forced liquid cooled	10–30	6500–20,000

Similarly, continuous TRV as:

$$TRV_{\text{cont}} = \frac{100}{\dfrac{\pi \cdot (0.55 \cdot 0.27)^2 \cdot 0.27 \cdot 0.8}{4}} \cdot 0.001 = 26.73\ \text{kN/m}^3$$

The above values suggest that we will select a sintered rare-earth permanent magnet machine, that will need forced liquid cooled system, while the overall dimensions of the machine can use a rotor diameter, D~150 mm, that is, 0.55 × 270 mm.

For axial length, we will select the value, L_{stk} = 150 mm, hence the machine rotor axial view will have a square profile ($D \sim L_{stk}$).

Assuming the ratio of stator and rotor dimensions is kept constant, increasing the rotor diameter will increase the stator slot depth, the electric loading, and the torque ratio per volume. Important advantages include smaller stator stack length, larger shaft diameter which implies large inertia and higher critical speed.

Similarly, under the same assumptions, the reduction on rotor diameter decreases the rotor inertia enhancing the dynamic response. Such configuration generates lower rotor mechanical stress at high speeds and reduces the end-turn copper losses. Lower diameter of the shaft implies smaller diameter for bearings which sustain higher speed operations at lower friction losses.

1.3.1 Stator and Rotor Topologies

When designing a brushless permanent magnet machine, there are several configurations that can be selected for stator and rotor assembly. At this stage, we do know the overall diameters and axial length only.

Rotor Magnetic Pole Pairs (p)

First step in further design procedure is to select the number of magnetic pole pairs. Based on the imposed maximum rotational speed, 15,000 rpm, and equation (1.9), it is possible to shortlist few suitable numbers. As derived from Table 1.4, we consider the maximum fundamental frequency to be 1000 Hz and this limits the suitable number of pole pairs to 1, 2, 3, and 4.

Considering the suitable number of pole pairs and the higher number of pole pair advantages:

- a higher torque ratio per volume due to the reduced leakage magnetic flux
- lower dimension of the stator back iron

TABLE 1.4 Variation of the fundamental frequency with number of pole pairs

Rotational speed (rpm)	Pole pairs	Poles	Fundamental frequency (Hz)
15,000	1	2	250
	2	4	500
	3	6	750
	4	8	1000
	5	10	1250
	6	12	1500

- reduced end-winding dimensions with implications on reduced copper losses and material consumption

However, higher number of poles generates higher permanent magnet resistive losses due to eddy-current effects induced in these conductive materials especially when magnets are mounted on the surface of the rotor.

Higher number of poles requires a short pole pitch which is well suited to use in concentrated windings. For distributed windings, the utilization of short pole pitch requires larger number of slots which can increase the mechanical vibrations, hence the acoustic noises.

The reluctance torque is proportional to the inductance of the winding which is inversely proportional to the square of the number of poles. Therefore, at higher number of poles the reluctance torque is significantly reduced.

Considering the advantages versus the disadvantages of higher specific core losses and converter losses due to higher frequency, still leads to the conclusion that the number of pole pairs equal to 4 is a good design choice.

Hence, we decide to have a rotor with four pole pairs (eight magnetic poles).

Rotor Poles Topology

The eight rotor poles can be designed with magnets mounted on the surface of the rotor (SPM—surface permanent magnet motor), or embedded in the rotor magnetic core (IPM—interior permanent magnet motor). For a traction application, the IPM topology has certain advantages as the magnet blocks can be of rectangular prism shape, better protected against demagnetization due to faults and high temperature profiles, and allows a more efficient field weakening operation.

The V-shape topology shown in Figure 1.7 is chosen.

Stator Number of Slots and Winding Topology

A balanced stator lamination and winding requires that certain rules are respected when deciding the number of slots:

- Slots/pole pairs >1 (no emf is possible otherwise)
- Slots/phases/parallel paths = Integer

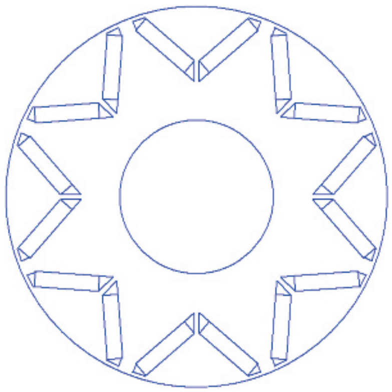

Figure 1.7 Eight-pole rotor topology.

- Pole pairs/parallel paths = $2k$, where k = Integer
- Slots/phases/greatest common divisor (GCD; Slots, pole pairs) = Integer

Following the above rules, a three-phase, 8-pole rotor can be paired with a stator with 12, 24, 36, 48, 72, 84, 96 slots.

In relation to the stator bore that is in the region of 150 mm, from the manufacturing point of view and cooling efficiency, **the number of stator slots is set to be 48**.

Figure 1.8 illustrates the proposed radial view of this electric motor design.

The winding is selected (as seen in Figure 1.9) to be:

- Three-phase, star connection
- Single coil layer (easier to implement and with high copper slot fill factor)

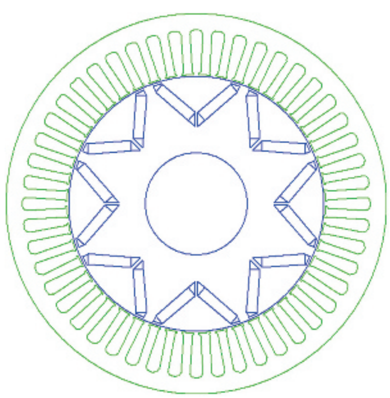

Figure 1.8 48 slots/8-pole IPM machine configuration.

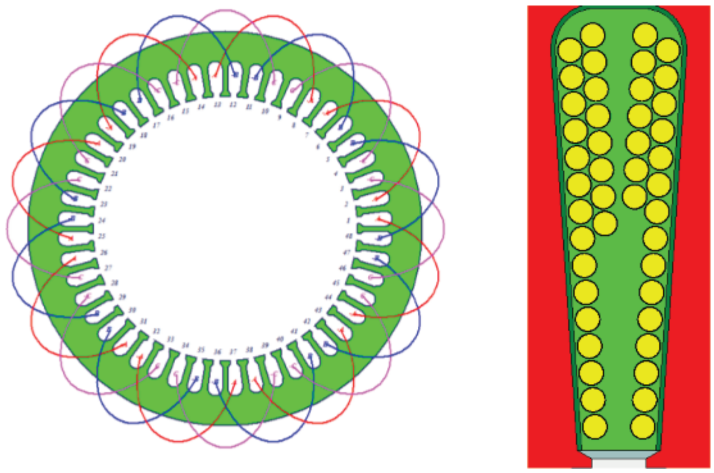

(a) (b)

Figure 1.9 (a) Winding pattern; (b) winding slot detail.

- Short pitch coil, that is, 1–6, compared to full pitch coil 1–7; this will eliminate certain higher-order harmonics
- Parallel paths (branches) are 2
- Turns/coil = 3
- Strands in hand = 7
- Wire gage = 1.3 mm

1.3.2 Drive Topologies

As schematically shown in Figure 1.10, either insulated gate bipolar transistors (IGBTs) or metal–oxide–semiconductor field-effect transistors (MOSFETs) are typical semiconductor devices used as switches on three-phase H-Bridge configurations.

The maximum peak line–line voltage equals the DC bus battery, and hence the maximum RMS line—line voltage $V_{\mathrm{RMS}} = V_{\mathrm{DC}}/\sqrt{2}$, where V_{DC} is the DC bus supply voltage. In reality, this is typically lower and dependant on modulation strategy.

The three-phase inverter controls the current by applying appropriate voltage at the machine terminals.

The terminal voltage must overcome the emf and voltage drop across the inductance to inject the correct voltage.

Field weakening is used to extend the speed range of the machine when the emf is greater than the maximum available terminal voltage.

Table 1.5 gives the ratio between inverter output RMS voltage and the input DC bus voltage for various pulse width modulation (PWM) control strategies.

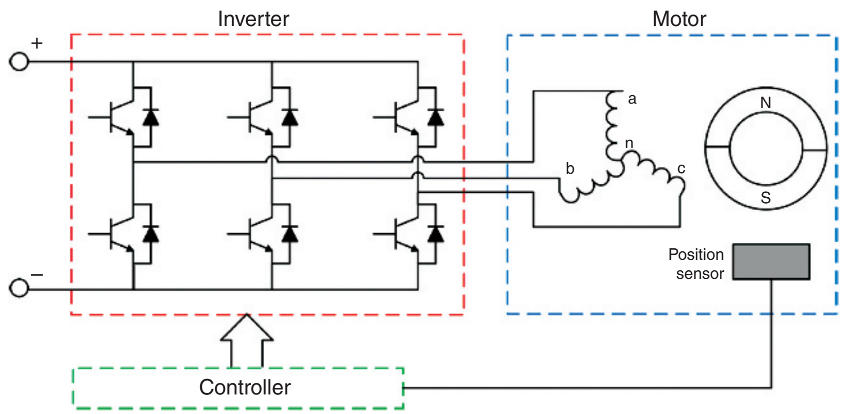

Figure 1.10 Electric drive topology of three-phase inverter, star-connected electric motor with controller.

1.3.3 Torque Speed Characteristics

In a wide speed range operation, the torque speed characteristics for IPM machines consist of three modes (Figure 1.11):

- In Mode I, the torque is limited by the current.
- In Mode II, the maximum current is used and the current angle is advanced to suppress the voltage.
- In Mode III, the current value converges toward the current value for theoretical infinite speed of λ_m/L_d, where λ_m is the rotor magnetic field and L_d is the D-axis inductance of the machine.

1.3.4 Electromagnetic Simulation Using Finite Element Analysis

The simulation presented has been achieved using ANSYS Maxwell which is capable of performing rigorous performance calculations of the machine including

TABLE 1.5 PWM strategy

PWM strategy	Line–line (RMS)/DC bus voltage ratio	Line–line (peak)/DC bus voltage ratio
Six-step 180	0.780	1.10
Hexagon tracking: piecewise linear	0.7446	1.05
Hexagon tracking: secant	0.7418	1.05
Third harmonic injection	0.707	1.00
Six-step 120	0.675	0.95
Maximum linear range of sine/triangle	0.612	0.87

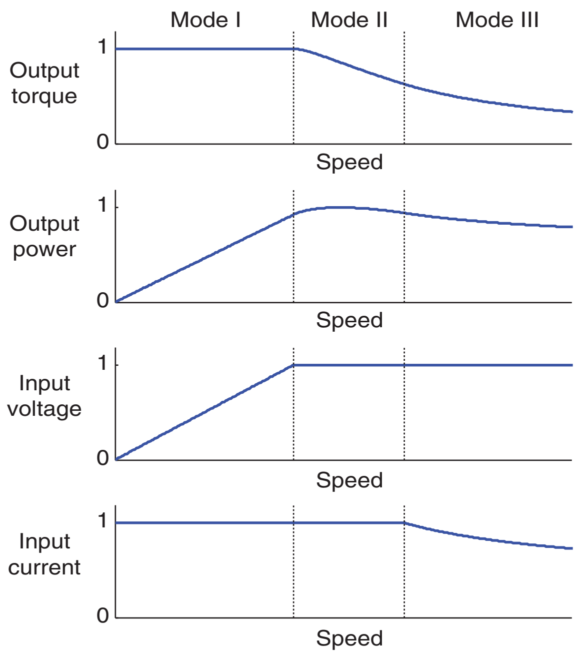

Figure 1.11 Operation modes in IPM machines.

the motion-induced physics caused by linear translational and rotational motion, advanced hysteresis analysis, demagnetization of permanent magnets and other critical electromagnetic machine parameters.

Starting exclusively on electromagnetic design flow narrowing the design space with ANSYS RMxprt, the magnetic transient design setup is automatically generated as either 2D or 3D designs. The benefit of 2D symmetry is due to radial magnetic field concept topology for most of electrical machines used in different applications. However axial field or transversal field topologies require 3D designs. Nevertheless, for accuracy reasons, 3D designs are required even if radial field topologies are considered when end effects, multiaxial segmented permanent magnets, or skewing topologies are employed. Although ANSYS Maxwell package is a general finite element analyses tool, its capabilities enable designers to customize and apply very specific analyses for electrical machines as D-Q solution computation (Figure 1.12), or employ even more complex algorithms as maximum torque per ampere unit (MTPA) control strategy (Figure 1.13) used to construct maps of efficiency and losses.

On the motor topology selected and sized based on the concepts developed in Section 1.3, we employed magnetic time-stepping (transient) analysis to predict more accurately the dynamic performance of such IPM design. Figure 1.14 shows field distributions on the surface of rotor and permanent magnets while Figure 1.15 and Figure 1.16 represent the transient data of running torque and induced voltage (back emf) profiles, respectively.

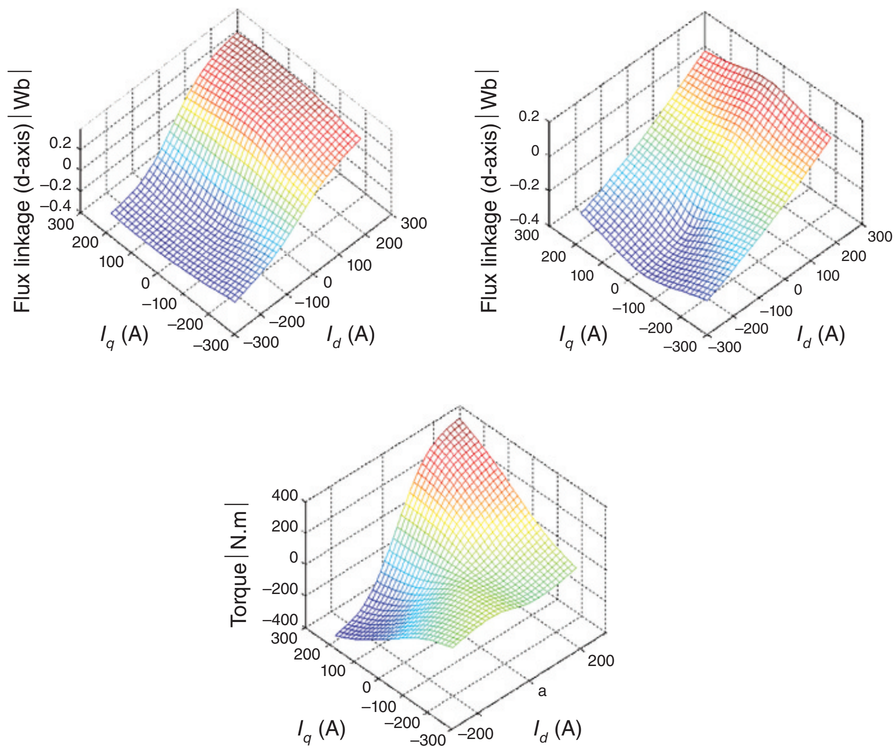

Figure 1.12 D-Q solution for interior permanent magnet machine design.

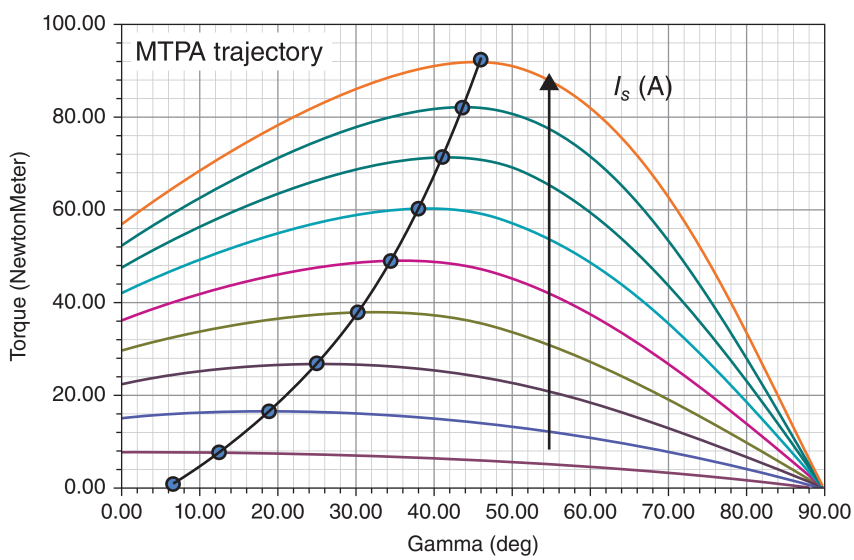

Figure 1.13 Maximum torque per ampere unit.

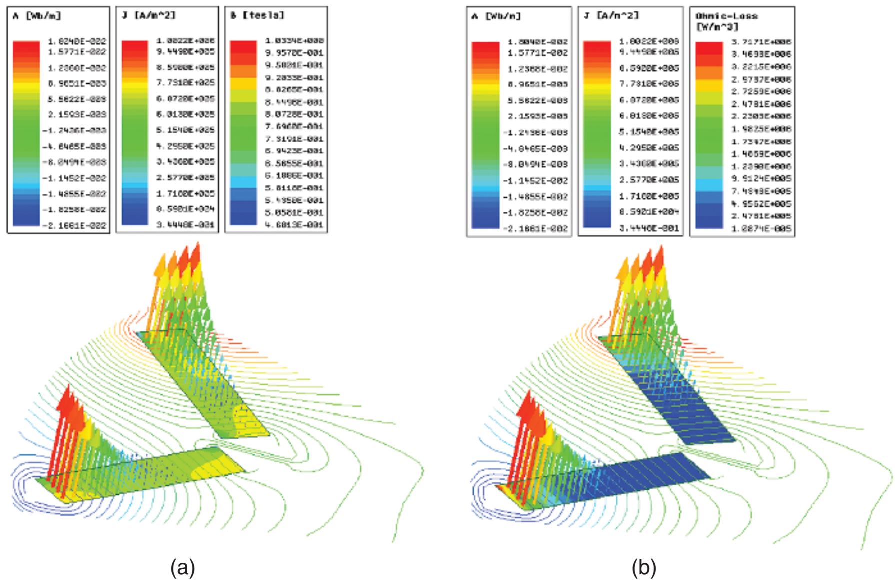

Figure 1.14 Field distribution on rotor and interior permanent magnets at the time instant of maximum input phase current:
(a) flux lines with magnetic field and induced current density distribution on PM,
(b) flux lines with power loss and induced current density distribution on PM.

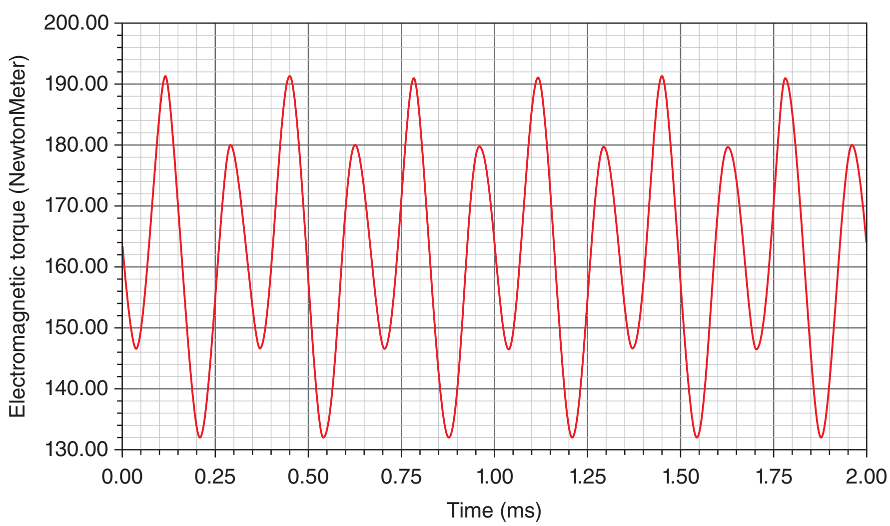

Figure 1.15 Electromagnetic torque characteristic.

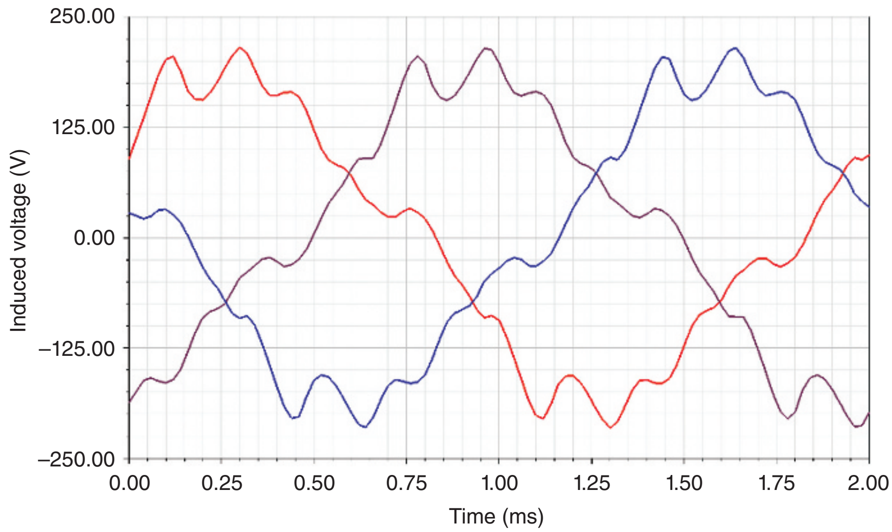

Figure 1.16 Induced voltage profile.

1.4 EFFICIENCY MAP

The AC brushless motors can be controlled using various control strategies. The most common strategies are:

- Maximum torque per ampere
- Maximum efficiency
- Unity power factor
- Constant phase advance angle, for example, $I_d = 0$, while $I_q =$ variable amplitude
- Constant power loss

The first two methods are described in Figure 1.17:

Maximum torque per amp		Maximum efficiency	
Minimize	$I_s = \sqrt{I_d^2 + I_q^2},$	Minimize	$W_{total} = W_{cu} + W_{fe} + W_{magnet},$
Subject to	$T_{shaft} - T_{demand} = 0$	Subject to	$T_{shaft} - T_{demand} = 0$
and	$V_{lim} \geq 2\pi f \sqrt{\psi_d^2 + \psi_q^2}.$	and	$V_{lim} \geq 2\pi f \sqrt{\psi_d^2 + \psi_q^2}.$

Figure 1.17 Control strategies for AC brushless PM machines.

Using MTPA control strategy and the power converter limits (V_{DC} = 400 V, I_{DC} = 500 A), it is possible to calculate torque–speed curves for the whole speed range. For each operation point, the following algorithms are considered:

- flux-linkages and inductances are calculated using 2D nonlinear transient finite element analysis model (e.g., ANSYS Maxwell)
- magnet losses are calculated considering the induced eddy-currents in the magnet blocks
- core losses are calculated via post-processing in finite element analysis with the flux-density distribution and applying statistical curves for the specific losses (e.g., Bertotti or Steinmetz models)
- Joule losses are calculated analytically for the DC component, and numerically for AC component based on finite element analysis
- mechanical/friction losses are determined using previous experience or measured data

With the amount of data created for the whole torque speed range, it is useful to display the loci of the efficiency isolines. These graphs are defined as efficiency maps and used to interpret the machine capability for entire operation spectrum, so that the designer can identify the speed and torque range where the efficiency is maximized, for example.

If the drive cycle is known, the operation points of this cycle can be superimposed on the efficiency map and thus observe if the machine was designed for optimal performance.

In automotive applications, there are standard drive cycles. Worldwide, the drive cycles presented in the Table 1.6 are representative:

TABLE 1.6 Standard drive cycles

Average speed	Distance	Time (s)	Description	Region	
19.59 mph	7.45 m	1369	Typical city driving conditions	USA	UDDS
48.3 mph	10.26 m	765	Typical highway conditions under 60 mph	USA	HWY
48.4 mph	8.01 m	569	High acceleration aggressive driving schedule	USA	US06
62.6 km/h	6.96 km	400	Extra-urban cycle	Europe	EUDC
59.5 km/h	6.6 km	400	Extra-urban (low powered vehicle)	Europe	EUDCL
18.4 km/h	0.99 km	195	Elementary urban cycle	Europe	ECE
17.7 km/h	0.66 km	135	10 mode cycle	Japan	JPN10
33.9 km/h	2.17 km	231	15 mode cycle	Japan	JPN15
25.6 km/h	6.34 km	892	Combined 10/15 mode cycle	Japan	JPN10.15

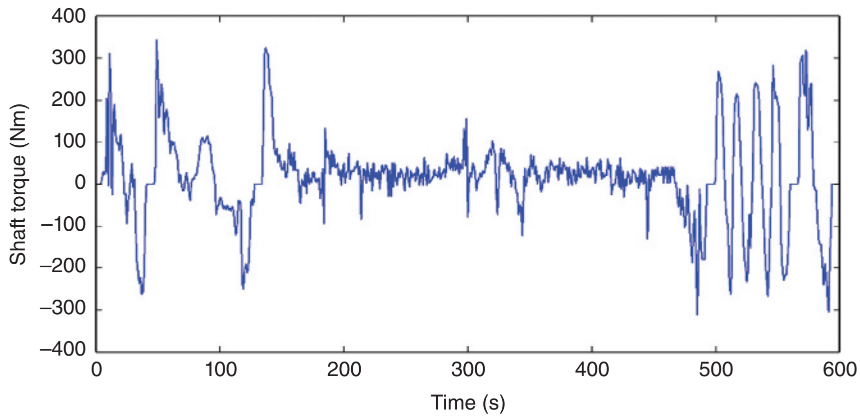

Figure 1.18 Torque variation in time for US06 drive cycle.

For the specific design in this chapter, we can consider the high acceleration aggressive drive cycle, US06 (USA). The detailed torque and power variation with rotational speed for this cycle are given in Figures 1.18 and 1.19.

Now, considering the ambient operation at 70°C and using the MTPA control strategy with flux-linkages and currents calculated with the electromagnetic model previously developed, the following efficiency maps can be plotted in both motoring and generating modes with drive cycle points superimposed. The efficiency map is generated in this example using the LAB module from Motor-CAD^{TM} software. The losses are extracted from ANSYS Maxwell 2D module.

Figure 1.20 shows a maximum efficiency of 96% in the region of 2000 rpm to 9000 rpm and up to 180 Nm. We notice that more than 60% of the driving points will be in the region with high efficiency.

For the base point, 100 Nm at 7500 rpm we get at the same fixed temperature of 70° as illustrated in Figure 1.21.

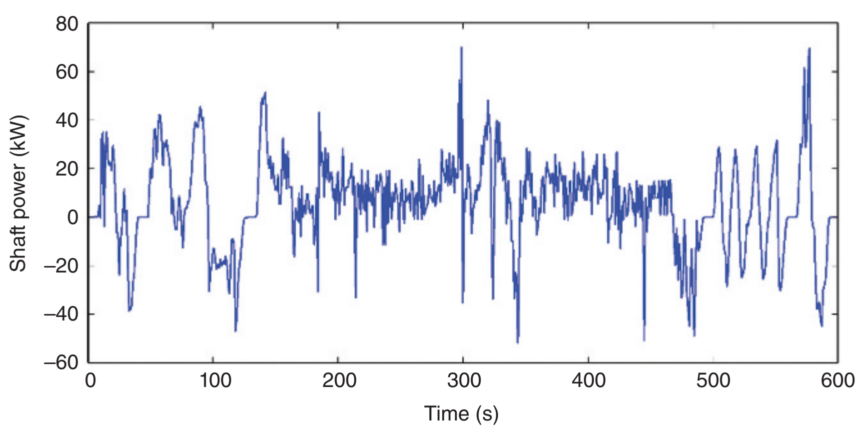

Figure 1.19 Shaft power variation in time for US06 drive cycle.

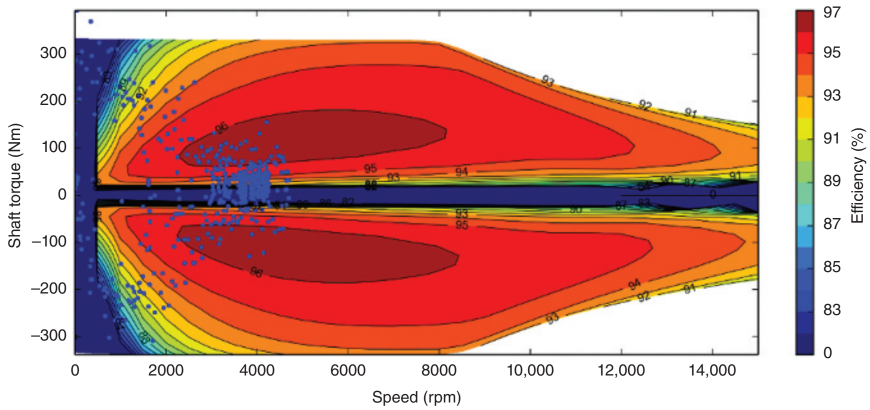

Figure 1.20 Efficiency maps in motoring and generating modes with superimposed US06 drive cycle points (blue dots).

Input Operating Point

Torque Required 100 Nm @ Speed 7500 RPM

Input:

◉ Torque ○ Maximum Current

Speed (rpm)	7500	Total Loss (W)	3270.95	Reluctance Torque (Nm)	15.6773
Shaft Torque (Nm)	99.9999	Copper Loss (W)	959.962	Terminal Power (kW)	81.8107
Shaft Power (kW)	78.5397	Iron Loss (W)	2127.84	Voltage (Vphase[rms])	123.533
Efficiency (%)	96.0018	Magnet Loss (W)	22.427	Power Factor	0.9171
Id (Arms)	-96.3233	Mechanical Loss (W)	160.714	Flux Linkage D (Vs)	0.03732
Iq (Arms)	220.598	Electromagnetic Power (kW)	80.8507	Flux Linkage Q (Vs)	0.04049
Phase Advance (Elec deg)	23.5883	Electromagnetic Torque (Nm)	102.942	Vd (Vphase[pk])	-127.945
Is (Arms)	240.711	Magnet Torque (Nm)	87.265	Vq (Vphase[pk])	118.958

Figure 1.21 Estimated electrical machine parameters for rated operation point in Motor-CAD / LAB module (100 Nm at 7500 rpm).

The results highlighted in Figure 1.21, show that about two-thirds of the losses are in the iron region, more specifically in the stator iron.

1.5 THERMAL CONSTRAINTS

In Section 1.4, we have seen the electrical machine capabilities for whole speed and current range, considering a fixed temperature of 70°C. This value would correspond to an ambient temperature in the engine compartment of an electrical vehicle.

When an electrical machine is designed for the required performance, the thermal response analysis is essential.

The main aspects are:

- The power output of an electrical machine is strongly affected by its thermal performance because machine operating temperature limits the electric loading, $q = f(I)$
- Machine life, with "10°C half-life rule", that is, every 10°C increase in operating temperature cuts insulation life by half
- Permanent magnet materials: the performance of magnets decreases with temperature as the magnets will be demagnetized if they are overheated
- Copper loss is temperature dependent
- Mechanical, elevated temperatures can induce mechanical stresses due to thermal expansion
- Bearing failure
- Thermal fatigue during variable speed operation

The losses in any electromagnetic device will generate heat. A good performance of an electrical machine relies on an efficient heat extraction to the ambient environment via one or more of the three main mechanisms: conduction, convection, and radiation (for more details, see Chpater 5, the dedicated chapter to thermal analysis)

The designed electrical machine example has a high torque per volume ratio (TRV) and most of the losses are located on the stator assembly (winding and laminated core). Hence, a good cooling system must use liquid forced convection. As illustrated in Figure 1.22, we can design a housing water jacket with spiral channels.

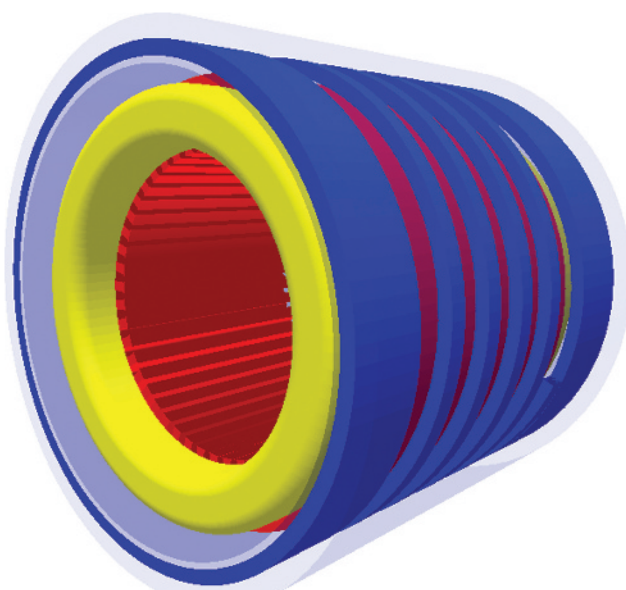

Figure 1.22 Three-dimensional view of the stator assembly and cooling jacket.

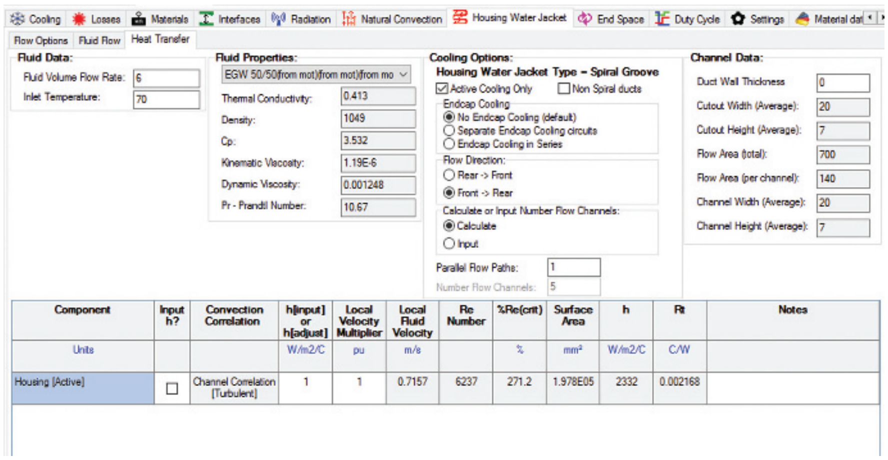

Figure 1.23 Cooling fluid flow and properties definition in Motor-CAD.

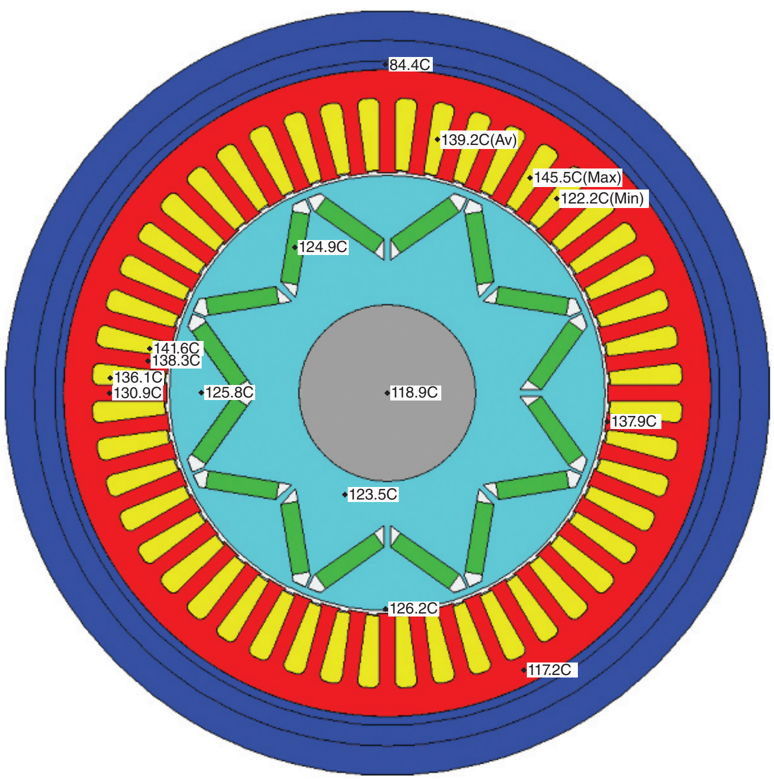

Figure 1.24 Radial view of the steady-state temperature distribution at 100 Nm at 7500 rpm operation point—based on thermal network.

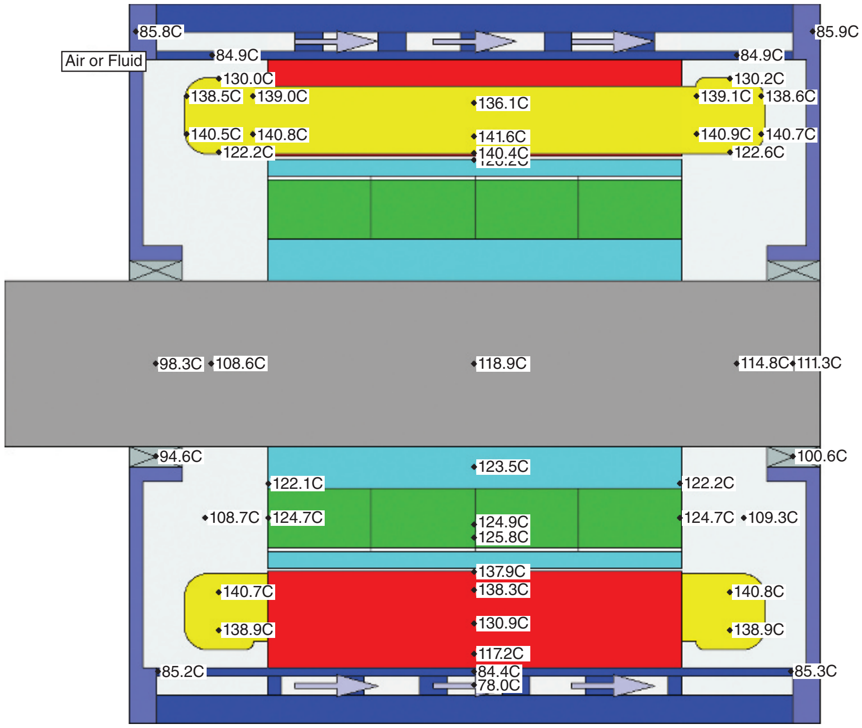

Figure 1.25 Axial view of the steady-state temperature distribution at 100 Nm at 7500 rpm operation point—based on thermal network.

Using Motor-CAD^{TM}, we can decide on the cooling channels' dimensions, on the cooling fluid, and the flow rate.

As observed in Figure 1.23, this machine is cooled using a housing spiral jacket with water ethylene–glycol mixture, 50–50%, fluid flow rate 6 L/min and inlet temperature of 70°C. The Reynolds number is 6237, which indicates a turbulent flow.

From Figure 1.24 to Figure 1.27, the thermal response at this load point will be using a lumped thermal network.

The computed characteristics reported in Figures 1.28–1.32 consider thermal envelope for continuous motor operation with maximum winding average temperature of 180°C and maximum permanent magnet average temperature of 140°C.

Figures 1.28–1.29 show that the proposed design is limited thermally by the magnet temperature.

1.6 ROBUST DESIGN AND MANUFACTURING TOLERANCES

Two important concepts for robust design and reliability analysis need to be introduced to better understand technical approaches will be further employed. To avoid

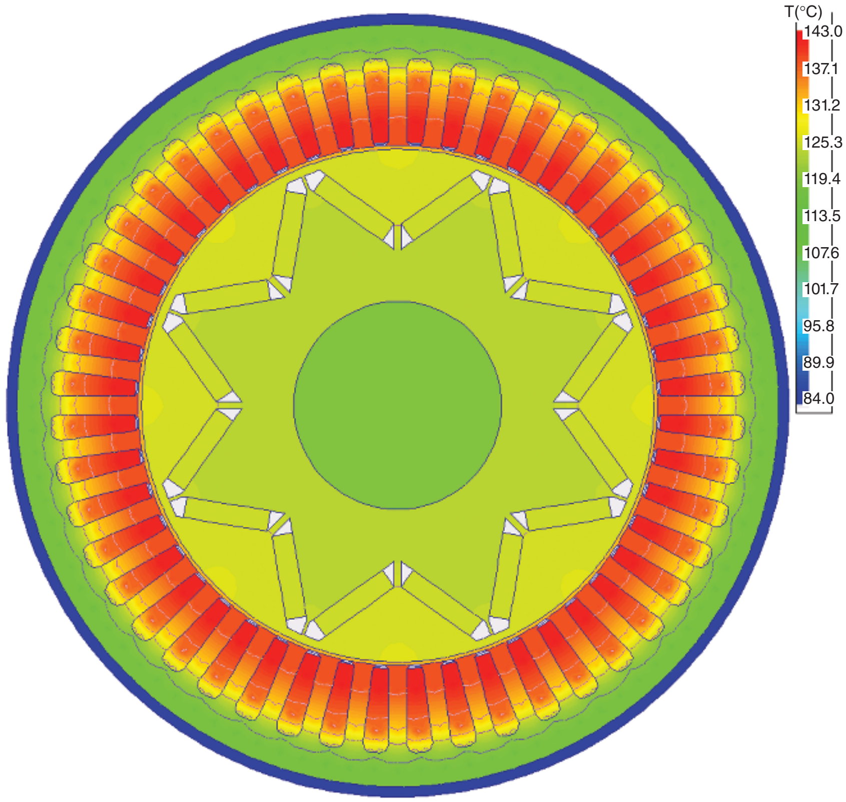

Figure 1.26 Radial view of the steady-state temperature distribution at 100 Nm at 7500 rpm operation point—finite-element thermal analysis.

further confusion, one can say that reliability analysis assesses the probability that various unpredictable design conditions yield unsustainable consequences, whereas robust design is the process based on which the required product specifications will be always satisfied in spite of variability and uncertainty.

Because a good design point is often the result of a trade-off between various objectives, the exploration of a given design cannot be performed by using optimization algorithms that lead to a single design point. It is important to gather enough information about the current design so as to be able to answer the so-called "what-if" questions, quantifying the influence of design variables on the performance of the product in an exhaustive manner. By doing so, the right decisions can be made based on accurate information, even in the event of an unexpected change in the design constraints.

For the sake of robust design representation on previously selected electric motor topology, Section 1.6.1 describes various simulation studies employing Design of Experiments (DOE), Response Surface, Parameter Correlation, Sensitivity and Six Sigma analyses.

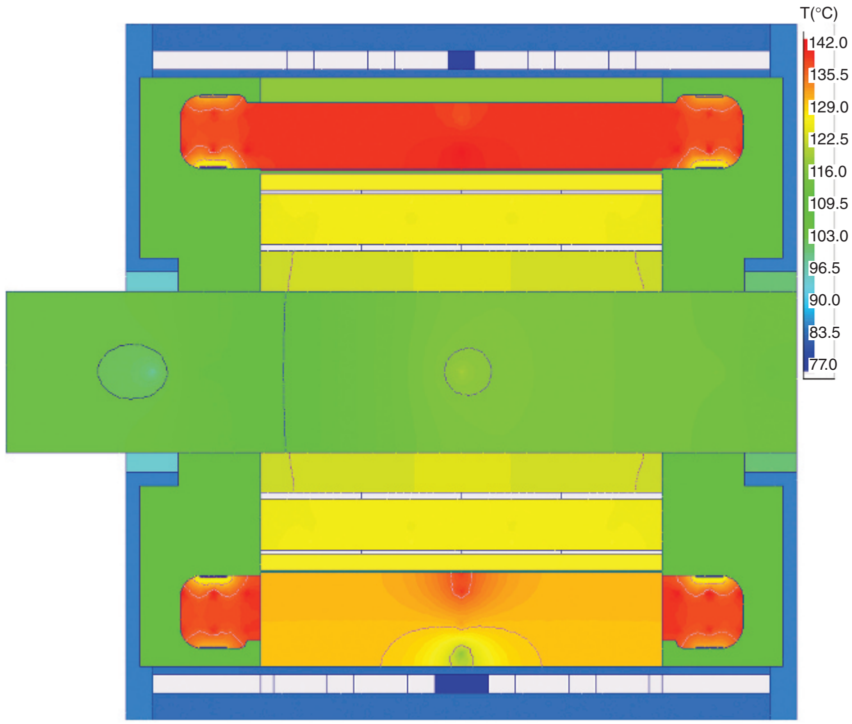

Figure 1.27 Axial view of the steady-state temperature distribution at 100 Nm at 7500 rpm operation point—finite-element thermal analysis.

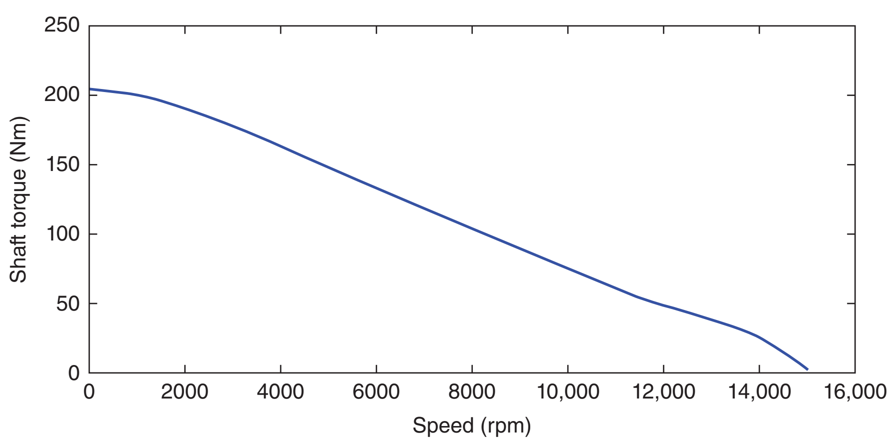

Figure 1.28 Continuous torque at average winding temperature <180°C and magnet temperature <140°C.

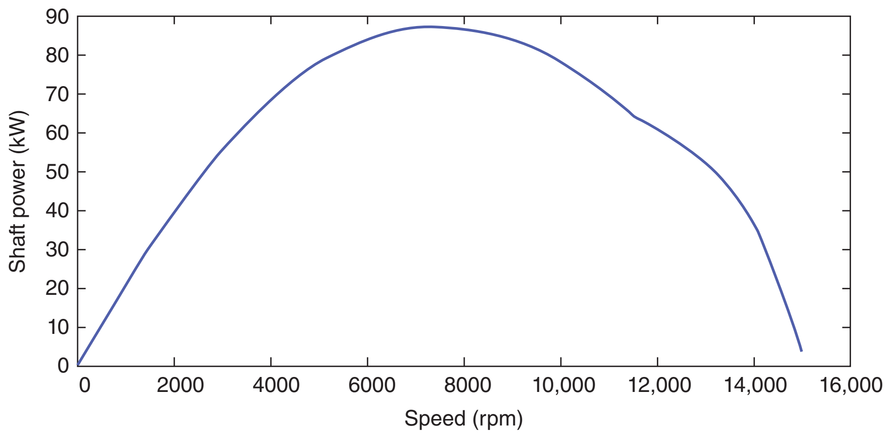

Figure 1.29 Continuous power at average winding temperature <180°C and magnet temperature <140°C.

1.6.1 Case Study

The proposed case study highlights meaningful steps on achieving robust design, enabling the engineers to account for uncertainties in product design and to determine how best to improve product reliability.

ANSYS Maxwell is used as finite element simulation tool to accurately predict the performance of the electric motor design while ANSYS Design Exploration provides with the robust design flow calling for an electromagnetic simulation on each design point defined by DOE. To ease the data transfer for enhancing the robust design with high level of flexibility, the flow highlighted in Figure 1.33 illustrates automatic connectivity among various components of the entire design analysis.

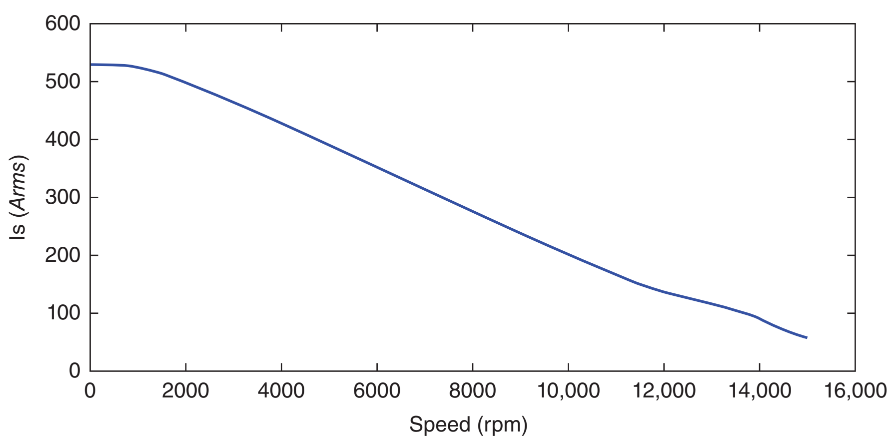

Figure 1.30 Continuous current at average winding temperature <180°C and magnet temperature <140°C.

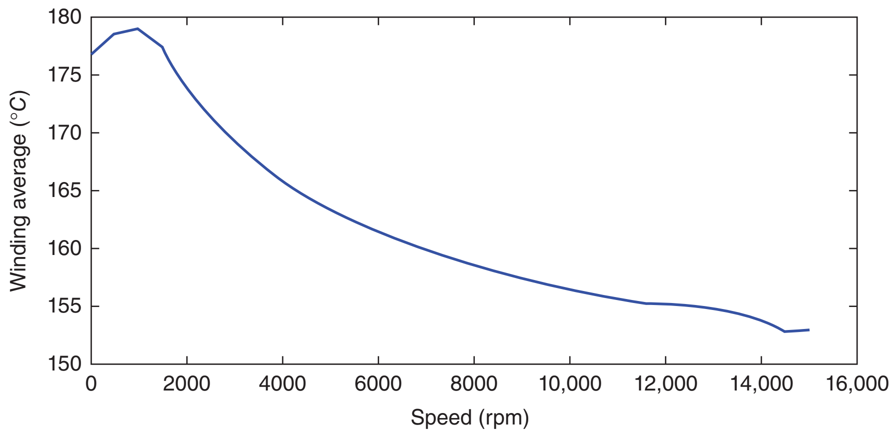

Figure 1.31 Average winding temperature variation with speed at steady-state thermal conditions.

To highlight the benefit of employing robust design analysis on electric machine design, the manufacturing tolerances are considered on the IPM motor topology highlighted in Tables 1.7 and 1.8.

Identify Key Design Parameters

The stator slot design has been selected (as seen in Figure 1.34) with parallel tooth configuration. Thus, only the top slot width (Bs2) varies while the bottom slot width (Bs1) is kept at a constant ratio of Bs2/Bs1 = 1.6. The rotor outer diameter as shown in Figure 1.34 will control the air-gap length, since the inner stator diameter (150 mm) is structurally constrained. The outer stator diameter is also fixed (220 mm) due to

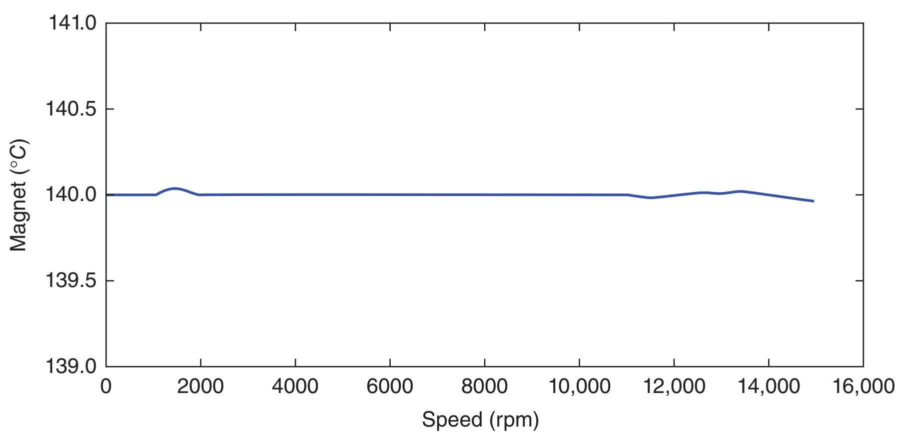

Figure 1.32 Magnet temperature variation with speed at steady-state thermal conditions.

housing and water jacket cooling configurations. Consequently, the stator slot height is fixed (22 mm) to maintain sufficient stator back iron thickness. A whole-coiled winding topology has been selected, as seen in Figure 1.35, with a fixed coil pitch (5) and 7 strands per conductor in two parallel branches distribution. Due to the minimum power density required to achieve the desired performance at base speed and maximum speed, both the length (50 mm) and width (6 mm) of IPM are fixed.

First part of such study describes the relationship between the design variables and the performance of the electric motor (Table 1.9) by using DOE, combined with Response Surface (RS). The main purpose of combined DOE with RS is to identify the relationship between the selected performance of the electric motor (P6 as average of electromagnetic torque and P7 as electromagnetic torque ripple) and the design variables (stator slot opening, stator slot width, air-gap length and the thickness of the IPM bridge). Practically, the design techniques are required to find the tolerance margins of the design variables in order to satisfy the optimized performance of the electric motor with certain confidence. Once the variation of the performance with respect to the design variables is known, it becomes easy to understand and identify all changes required to meet the requirements for the electric motor. For instance, once the response surfaces are created, the information can be shared in easily understandable terms: curves, surfaces, sensitivities. They can be used at any time during the development process without requiring additional simulations to test a new motor design instance.

Design of Experiments and Response Surface Analysis

In a process of engineering design, it is very important to understand what and how many input variables are contributing factors to the output parameters of interest. It is a lengthy process before a conclusion can be made as to which input variables play a role in influencing the output parameters. Designed experiments help revolutionize the lengthy process of costly and time-consuming trial-and-error search to a powerful and cost-effective statistical method.

A very simple designed experiment is screening design. In this design, a permutation of lower and upper limits of each input variable is considered to study their effect to the output parameters of interest. While this design is simple and popular in industrial experimentations, it only provides a linear effect, if any, between the input variables and the output parameters. Furthermore, effect of interaction of any two input variables, if any, to the output parameters is not characterizable.

To compensate for the insufficiency of the screening design, it is enhanced to include center point of each input variable in experimentations. The center point of each input variable allows a quadratic effect, minimum or maximum inside explored space, between input variables and output parameters to be identifiable, if one exists. The enhancement is commonly known as response surface design to provide quadratic response model of responses. The quadratic response model can be calibrated using full factorial design (all combinations of each level of input variable) with three or more levels. However, the full factorial designs generally require more samples than necessary to accurately estimate model parameters. In

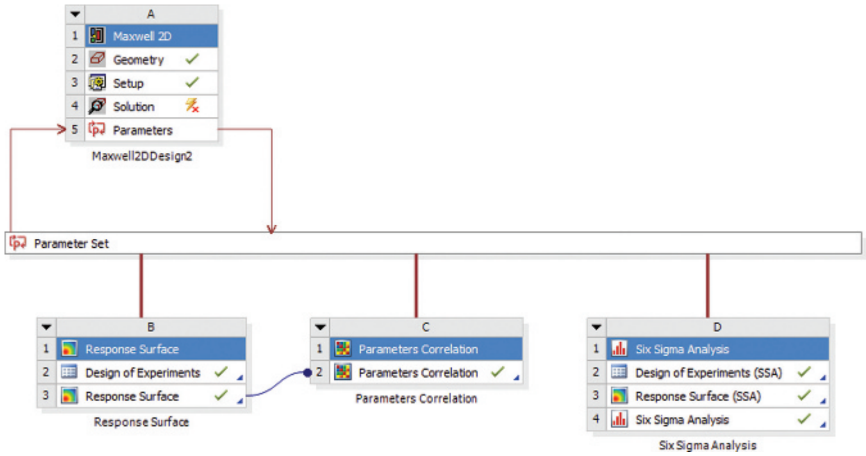

Figure 1.33 ANSYS workflow on robust design analysis based on ANSYS Maxwell as finite element analysis solution.

TABLE 1.7 IPM specifications

Performance *s*pecification	Values
DC *b*us	400 V
Peak *t*orque	330 Nm
Peak *p*ower	235 kW
Max *s*peed	15,000 rpm
Base *s*peed	7500 rpm
Continuous *p*ower at *b*ase *s*peed	80 kW
Continuous *t*orque at *b*ase *s*peed	100 Nm

TABLE 1.8 IPM dimensions

Motor design details	Values
Slots	48
Poles	8
Stator OD	220 mm
Stator *a*xial *l*ength	150 mm
Axial laminated pack	150 mm
Stator and *r*otor *s*teel	M270-35A
Permanent magnets	N38UH (Br = 1.05 T and Hc = 360 kA/m at 70°C)

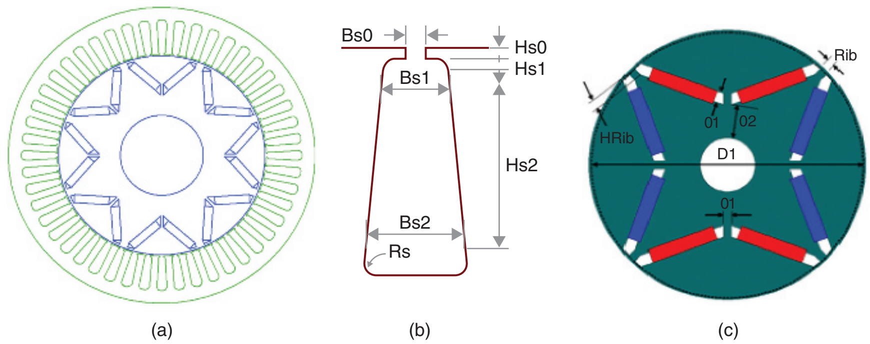

Figure 1.34 Electric motor design topology: (a) IPM 2D-cross section; (b) stator slot dimensions; (c). IPM rotor dimensions.

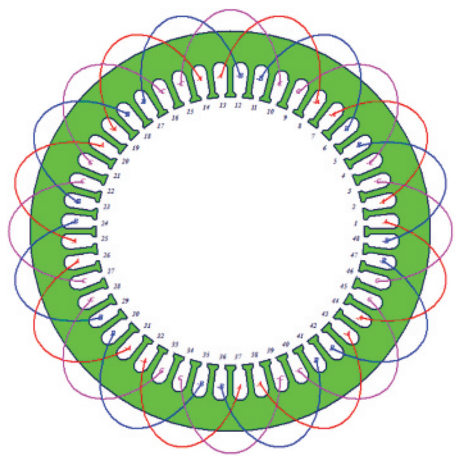

Figure 1.35 A whole-coiled winding topology.

light of the deficiency, a statistical procedure is developed to devise much more efficient experiment designs using three or five levels of each factor but not all combinations of levels, known as fractional factorial designs. In this study among these fractional factorial designs, the most popular response surface designs known as Central Composite Design (CCD) is used.

TABLE 1.9 Design parameters definition

Design variables (Parameters)	Description	Initial values
P2 (Bs0)	Stator slot opening (mm)	3
P3 (Bs2)	Top stator slot width (mm)	7
P4 (OD)	Rotor outer diameter (mm)	146
P5 (Rib)	PM bridge (mm)	1

TABLE 1.10 Design variable with lower and upper bounds

Design variables	Lower bound (LB)	Upper bound (UB)
P2 (BS0) (mm)	1	4
P3 (BS2) (mm)	6	8.5
P4 (OD) (mm)	146	148.5
P5 (RIB) (mm)	1	5

In fact, DOE is a technique used to determine the location of sampling points and is included as part of the Response Surface and Six Sigma systems. There are several versions of DOE available in engineering literature. These techniques all have one common characteristic: they try to locate the sampling points such that the space of random input parameters is explored in the most efficient way, or obtain the required information with a minimum of sampling points. Sample points in efficient locations will not only reduce the required number of sampling points, but also increase the accuracy of the response surface that is derived from the results of the sampling points. By default, the deterministic method uses a CCD, which combines one center point, the points along the axis of the input parameters, and the points determined by a fractional factorial design.

The design variables selection is presented in Table 1.10 where for each variable both lower bound and upper bound are identified. The computed minimum and maximum for selected output parameters are shown in Table 1.11. Based on the CCD, the DOE creates and solves only the design points presented in Figure 1.36.

This analysis generates the data required by Response Surface analysis. The first result of Response Surface analysis, Goodness of Fit that shows how well the Response Surface data prediction fits the expected results observed from design points is illustrated in Figure 1.37. The Goodness of Fit summarizes the difference between observed values and the values expected. In the current case study, it tests whether two samples are drawn from identical distributions.

Figure 1.38 shows local sensitivity plot for all design variables with respect to both output parameters. Important to mention is the positive sensitivity of stator slot width (P3 design variable) with respect to ripple torque (P7) and negative sensitivity with respect to average torque (P6). This analysis shows that with decreasing stator slot width the average torque increases while torque ripple decreases. This is a

TABLE 1.11 Output parameters' description

Output parameters	Calculated minimum	Calculated maximum
P6 average torque (Nm)	130.51	173.5
P7 torque ripple (%)	3.18	13.83

	A	B	C	D	E	F	G
1	Name	P2 - x1 [mm]	P3 - x2 [mm]	P4 - x4 [mm]	P5 - x5 [mm]	P6 - mean(Moving1.Torque)	P7 - ripple(Moving1.Torque)
2	1	2.5	7.25	147.25	3	151.95	6.1393
3	2	1	7.25	147.25	3	152.45	4.8273
4	3	4	7.25	147.25	3	149.69	9.3654
5	4	2.5	6	147.25	3	157.69	5.3515
6	5	2.5	8.5	147.25	3	141.86	7.5277
7	6	2.5	7.25	146	3	134.59	4.2139
8	7	2.5	7.25	148.5	3	168.12	9.7478
9	8	2.5	7.25	147.25	1	144.08	4.9175
10	9	2.5	7.25	147.25	5	155.56	6.2703
11	10	1.4437	6.3697	146.37	1.5916	139.39	3.5572
12	11	3.5563	6.3697	146.37	1.5916	136.77	4.9217
13	12	1.4437	8.1303	146.37	1.5916	131.98	4.3963
14	13	3.5563	8.1303	146.37	1.5916	130.51	5.7024
15	14	1.4437	6.3697	148.13	1.5916	164.09	5.5889
16	15	3.5563	6.3697	148.13	1.5916	163.12	7.1734
17	16	1.4437	8.1303	148.13	1.5916	150.4	7.3814
18	17	3.5563	8.1303	148.13	1.5916	149.58	9.1663
19	18	1.4437	6.3697	146.37	4.4084	145.58	3.1781
20	19	3.5563	6.3697	146.37	4.4084	142.77	6.1977
21	20	1.4437	8.1303	146.37	4.4084	137.83	4.1625
22	21	3.5563	8.1303	146.37	4.4084	136.17	7.233
23	22	1.4437	6.3697	148.13	4.4084	173.5	6.0555
24	23	3.5563	6.3697	148.13	4.4084	173.03	10.728
25	24	1.4437	8.1303	148.13	4.4084	158.72	9.4615
26	25	3.5563	8.1303	148.13	4.4084	157.77	13.832

Figure 1.36 Design of Experiments creates a reduced parametric table for further robust design analysis.

critical observation when attempting to reduce torque ripple and increase average torque in the same time. Similarly, the effect of slot opening (P2) has larger impact (positive sensitivity) on torque ripple generation than average torque production (negative sensitivity). The air-gap length controlled by outer rotor diameter (P4) shows positive sensitivity on both average torque and ripple torque predictions. This analysis tremendously helps to decide appropriate design variables for further optimization process.

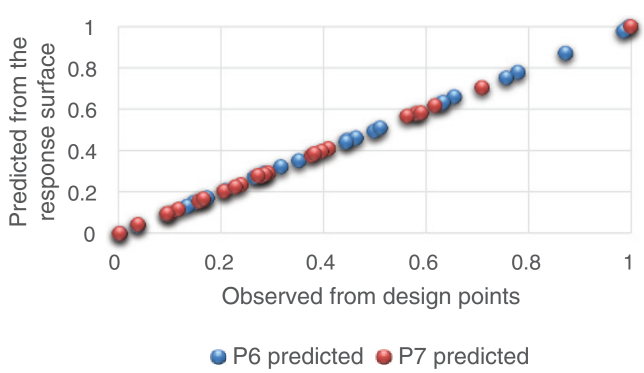

Figure 1.37 Goodness of Fit representation based on Response Surface analysis.

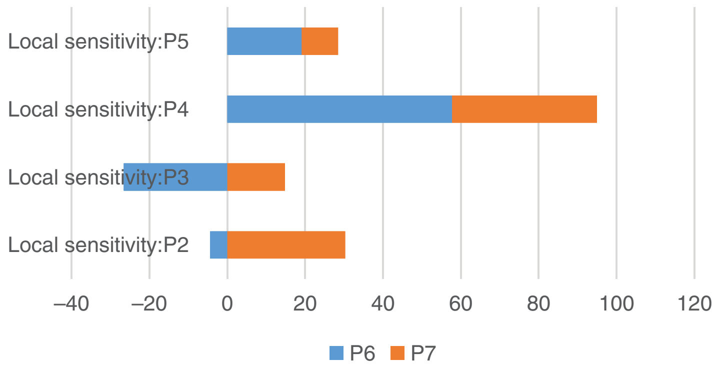

Figure 1.38 Local sensitivities for selected design variables with respect to defined output parameters.

Response Surface analysis builds 3D surface plots (Figure 1.39) illustrating average torque and ripple torque variations as function of slot opening (P2) and outer rotor diameter (P4) input design variables. Similarly, the 3D surface plots (Figure 1.40) show the surface variation of average torque and ripple torque, respectively as function of stator slot width (P3) and outer rotor diameter (P4).

At this stage of Response Surface analysis if design optimization is employed, one can further investigate the feasibility of the optimized design points with respect to imposed constraints. A screening method is used to build a trade-off analysis using 2000 evaluations to represent the feasible design points as Pareto chart or trade-off plot (Figure 1.41).

Pareto fronts search has been performed to investigate the feasible design points for further statistical studies considering tolerances. In this case study, the two defined goals are to reduce the ripple torque and increase the running torque. In such a case, one goal may be realized at the expense of the other.

The trade-off plot shows the line along which no improvement in one parameter's goal can be achieved without sacrificing the other (Pareto optimal). Pareto or non-dominated set, is a group of solutions such that selecting any one of them in place of another will always sacrifice quality for at least one objective, while improving at least one other.

Among all feasible design points, the optimized design point has been selected (Tables 1.12 and 1.13) by weighting the contribution of individual goals. In this study, ripple torque assumes higher contribution to the optimized design decision-making whereas running torque should be larger than 160 Nm.

Six Sigma Design

A Six Sigma analysis determines the extent to which uncertainties in the model affect the results of an analysis. An uncertainty (or random quantity) is a parameter whose value is impossible to determine at a given point in time (if it is time-dependent)

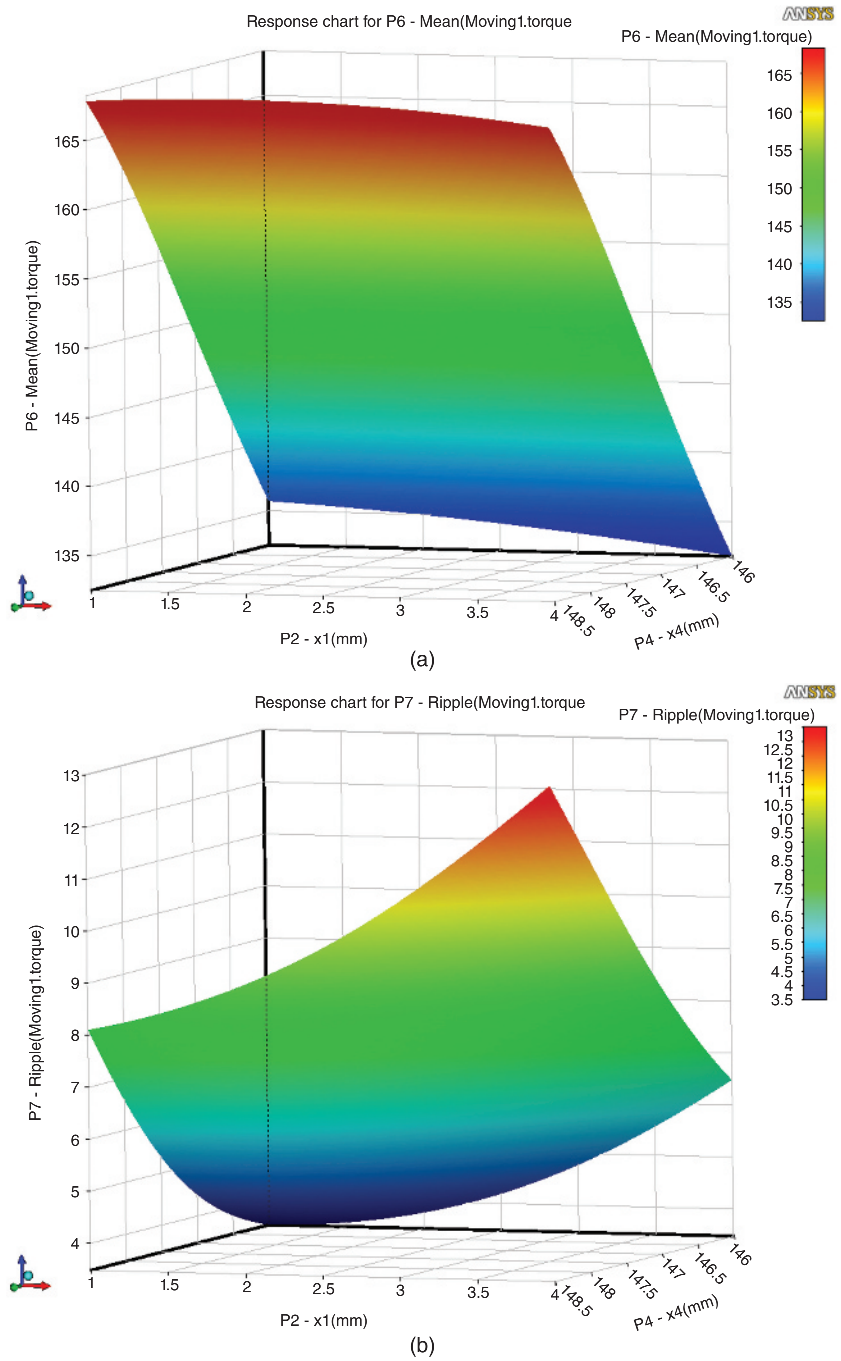

Figure 1.39 Three-dimensional surface plots: output parameters versus input design variables. (a) Average torque-P6 versus P2 and P4; (b) Ripple torque-P7 versus P2 and P4

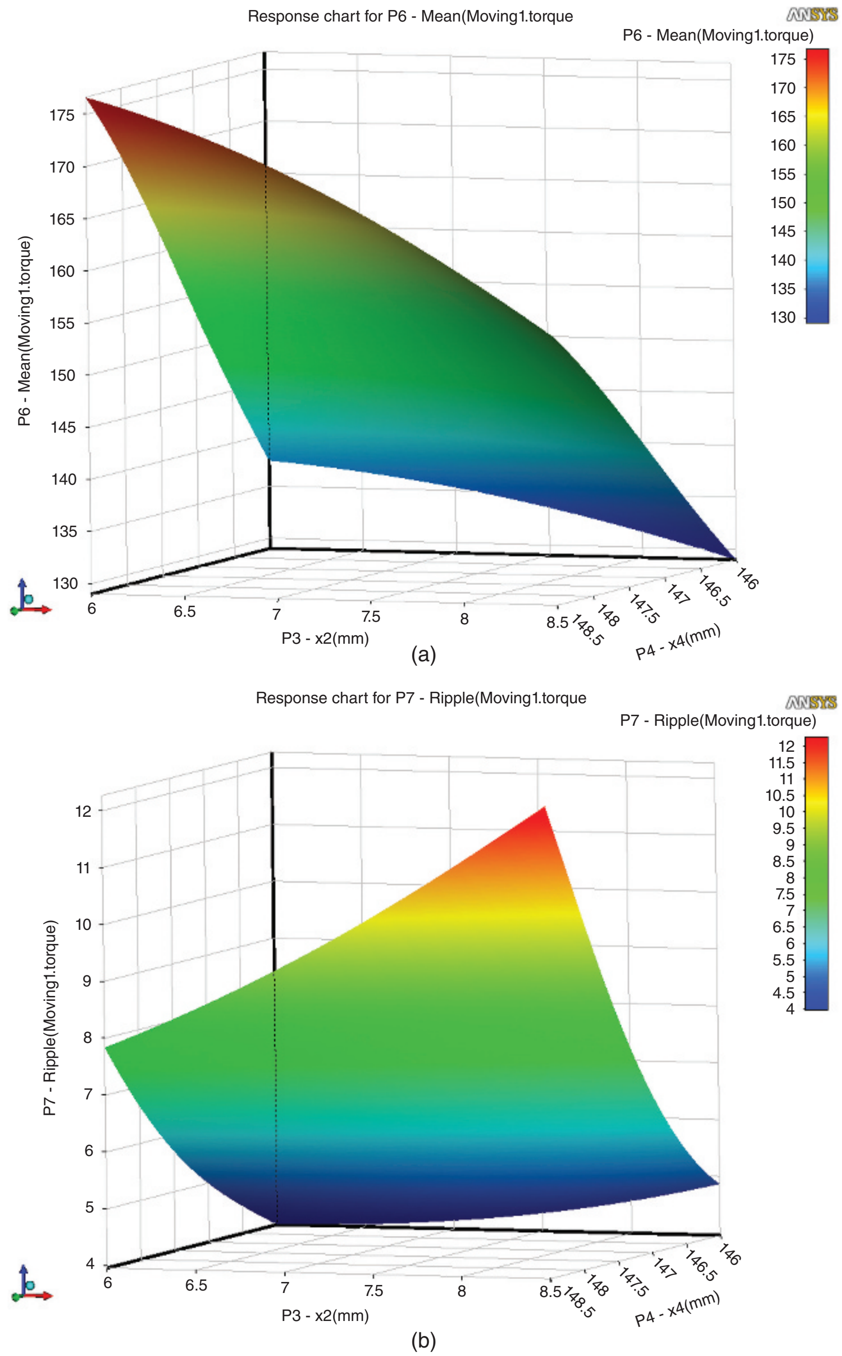

Figure 1.40 Three-dimensional surface plots: output parameters versus input design variables. (a) Average torque-P6 versus P3 and P4; (b) Ripple torque-P7 versus P3 and P4

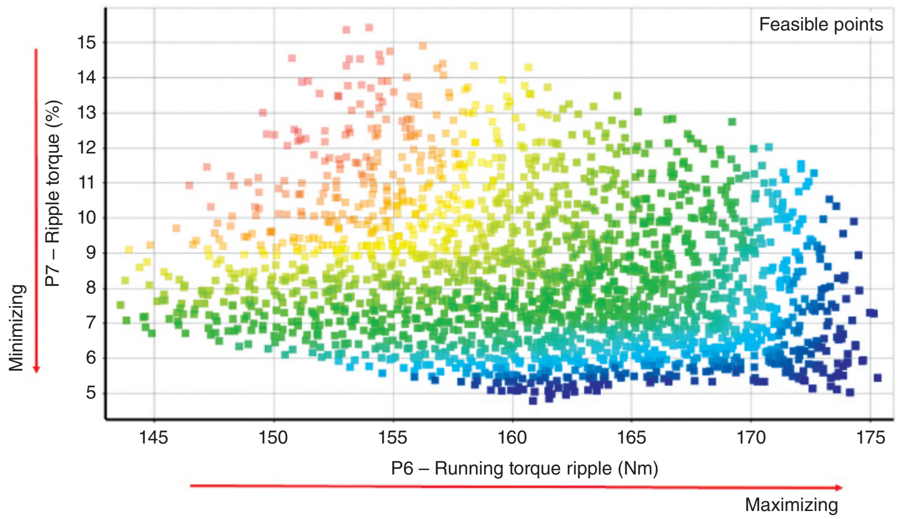

Figure 1.41 Pareto front search.

or at a given location (if it is location-dependent). There have been published some significant works on motors and drives considering Six Sigma process [9–16].

A Six Sigma analysis uses statistical distribution functions (such as the Gaussian, or normal distribution, the uniform distribution, lognormal, etc.) to describe uncertain parameters. By means of simulations one can measure numerically predicting the performance of a device or product. To assess the quality of such performance, Six Sigma analysis determines whether the design satisfies Six Sigma quality criteria. In fact, Six Sigma analysis is a statistical analysis, which when applied to a simulation generates a test of significance against the criteria of the device good quality.

TABLE 1.12 Optimized design variables

Design variables	Optimized value
P2 (BS0) (mm)	1.17
P3 (BS2) (mm)	6.08
P4 (OD) (mm)	148
P5 (RIB) (mm)	3.3

TABLE 1.13 Optimized motor design performance

Output parameters	Optimized performance
P6 average torque (Nm)	170.58
P7 torque ripple (%)	5.2673

In general, considering μ the mean of a large population with σ the population standard deviation, $\bar{x}$ the mean of a simple random sample of the population which obeys normal distribution in order to apply the central limit theorem (CLT), one can easily predict the margin errors (tolerances) estimating the population mean with certain confidence level. In this case, the confidence interval (CI) can be calculated by

$$\bar{x} \pm z^* \frac{\sigma}{\sqrt{N}}, \tag{1.11}$$

where N is the size of sample and z^* is a parameter given by the selected confidence level.

In statistics, the very well-known *68-95-99.7* rule provides with the confidence levels in terms of probabilities of values that lie within a band around the mean in a normal distribution with a width of two, four, or six standard deviations. The data outside of these intervals do not obey the quality criteria, in other words, for such design variations the device or product fails to sustain the level of desired performances. For example, if the confidence level of the desired quality is 99.7% then only 1−0.997 = 0.003 or almost 3000 parts out of every 1 million manufactured fail. Similarly, a product has Six Sigma quality—with the confidence level as high as 99.99966%—if only 3.4 parts out of every 1 million manufactured fail. This quality definition is based on the assumption that an output parameter relevant to the quality and performance assessment follows a Gaussian (normal) distribution, as shown in Figure 1.42.

The main goal of this study is to assess the design fitness based on Six Sigma analysis on selected electric motor topology. Considering the level of confidence as

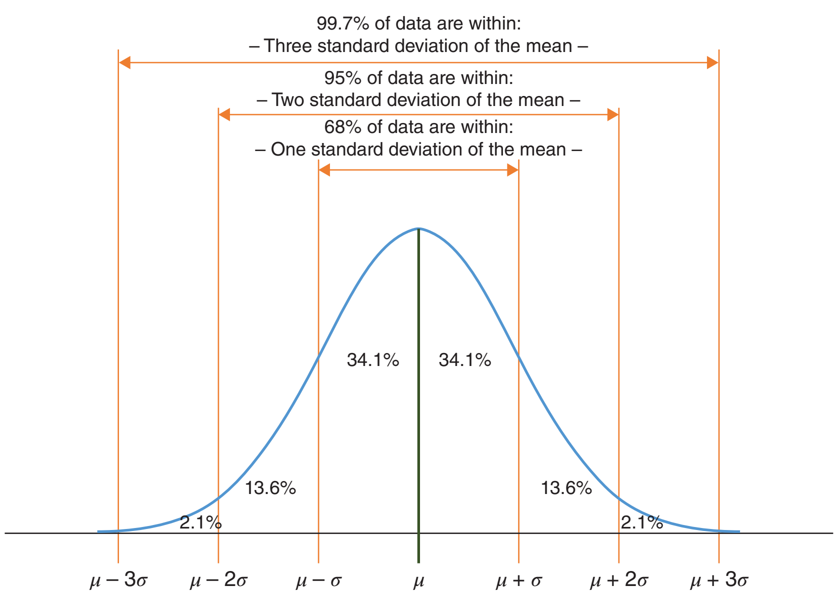

Figure 1.42 Normal distribution parameters and their graphical representation.

99.7%, the confidence interval is $\mu \pm 3\sigma$. Assuming the mean of population as the mean of individual simulations (sample) for each design variable, one can easily calculate the individual simulation standard deviation as

$$\mu \pm 3\sigma = \mu \pm \Delta x \cdot \mu \tag{1.12}$$

where Δx could be interpreted as the tolerance value for corresponding design variable. Then one can assume

$$\sigma_x = \frac{\Delta x \cdot \mu}{3} \tag{1.13}$$

where σ_x represents the standard deviation of individual samples.

In this study, the optimized IPM design topology is selected according to Response Surface analysis. Based on this assumption, the design variables corresponding to P2, P3, P4, and P5 are selected as baseline design variables that provide with high torque profile and low ripple torque characteristic. Statistically, the values of the Response Surface output parameters are considered to be the parameters of the population. In such condition, these values are used to test the statistical significance when Six Sigma analysis is performed. Although the design variable P4 that controls air-gap length is set fixed at 148 mm providing with an air-gap length of 1 mm, all other design variables are introduced assuming their nominal values obey normal distribution with mean values corresponding to the optimized design point and standard deviations calculated based on tolerances as described in (1.13) and shown in Table 1.14. Considering the tolerances of design variables as 3σ, one can calculate the simulated design variables' standard deviations at given uncertainty 10%, 5%, and 1%, respectively. The uncertainty of design variable can change the performance of the electric motor. The main goal is to use such design variable distribution to estimate the variation band of the output parameters according to the uncertainty.

Based on this table, Six Sigma can combine different standard deviations for individual design variables to control the variation band of the output parameters. An iterative procedure might be applied using Six Sigma analysis to increase the test of significance ensuring high quality design and in the same time to balance the cost of generating such quality. At each iteration, these values are selected based on sensitivity analysis which shows which design variable variation has more effect on selected output parameters. The importance of such analysis relates very well to the manufacturing tolerance process [17] providing with the level of confidence if the electric motor will run at the targeted performance.

TABLE 1.14 Design variable tolerances

Design variables	Mean value	STD. deviation at 10% uncertainty	STD. deviation at 5% uncertainty	STD. deviation at 1% uncertainty
P2 (BS0) (mm)	1.17	0.039	0.0195	0.0039
P3 (BS2) (mm)	6.08	0.203	0.101	0.0203
P5 (RIB) (mm)	3.3	0.11	0.055	0.011

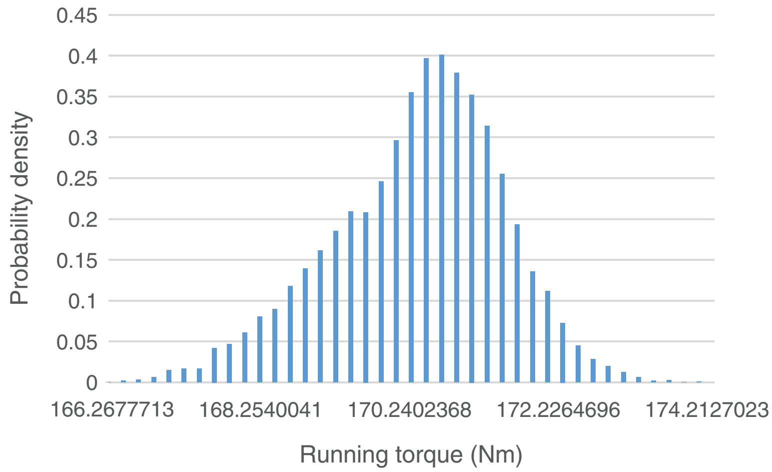

Figure 1.43 Running torque distribution on 10%-10%-10% design variable tolerances.

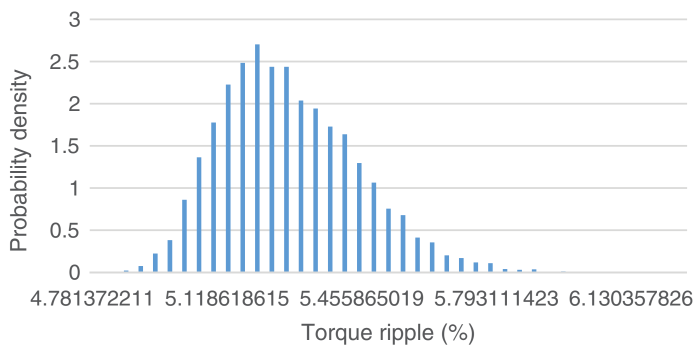

Figure 1.44 Torque ripple distribution on 10%-10%-10% design variable tolerances.

If Six Sigma analysis is performed with a tolerance of 10% for all design variables (P2, P3, P5) based on 3σ level (Table 1.15), the variation of individual output parameters as statistical distribution is shown in Figures 1.43 and 1.44.

The distributions of running torque (which is the average torque of electric motor at steady state) and torque ripple show following statistics:

TABLE 1.15 10%-10%-10% tolerances on design variables

10% tolerance on P2 10% tolerance on P3 10% tolerance on P5	Mean value	Probability value
Running torque (Nm)	170.24	0.4874 (P > 170.58 Nm)
Ripple torque (%)	5.456	0.6025 (P < 5.2673%)

In Table 1.15, "mean value" represents the mean for Six Sigma simulation whereas "probability value" represents the probability which is a hypothesis testing procedure based on the z-statistic. In this case study for given hypothesized population mean, this is the probability that the sample mean would be greater or less than the average of simulations statistically seen as observed data. In this context, the probability will measure the acceptance levels that the value corresponding to running torque will be greater than the optimized value of 170.58 Nm and the value corresponding to torque ripple will be less than the optimized value of 5.2673%. As an important note in these results there is no significant skewness (mean value practically is equal to median value). This observation is valid for entire study presented in this section.

The probability value can be also evaluated using z-test computed as

$$z^* = \frac{\bar{x} - \mu}{\sigma / \sqrt{N}} \tag{1.14}$$

Using (1.14), one can calculate the probabilities of higher or smaller values using the standard normal distribution table as a $P(z > z^*)$ for running torque and $P(z < z^*)$ for torque ripple.

According to this analysis, almost 60.25% of all designs will have torque ripple values less than 5.2673%. Similarly, almost 48.74% of all designs will have running torque values greater than 170.58 Nm. Since the running torque level of confidence could use higher error margins, the main goal is to provide with higher sigma-level confidence on ripple torque prediction.

In order to reduce scatter of the outputs, selection of design variables requires smaller tolerances. To select the appropriate design variable, sensitivity analysis is performed as shown in Figure 1.45.

This analysis shows that the design variable related to slot width (P3) has major impact on both running torque and torque ripple. Basically, P3 design variable

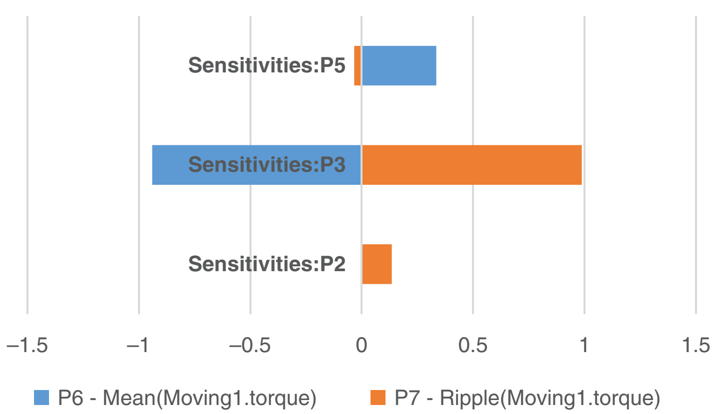

Figure 1.45 Sensitivity results for 10%-10%-10% design variable tolerances.

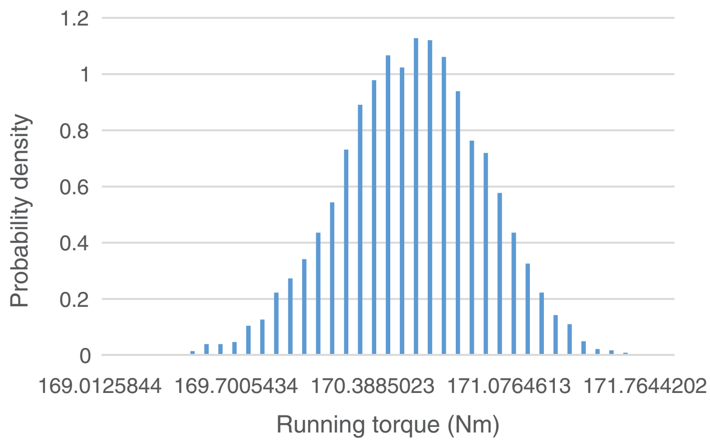

Figure 1.46 Running torque distribution on 10%-10%-1% design variable tolerances.

exercises opposite sensitivities on running torque. Therefore, the shown positive sensitivity illustrates that any decrease on slot width will generate a decrease in the ripple torque value whereas highlighted negative sensitivity demonstrates that any decrease on slot width will generate an increase in running torque value. This is an excellent example to show sensitivity analysis when a design variable needs to be selected for further optimization. In this study, practically a reduction of the slot width value will increase the torque and reduce the torque ripple. Therefore, a lower tolerance (1%) is considered for design variable P3.

Six Sigma analysis is then performed with a tolerance of 10% for design variables P2 and P5 and 1% tolerance for design variable P3 based on same 3σ level. Figures 1.46 and 1.47 illustrate the new distribution of running torque and torque ripple characteristics.

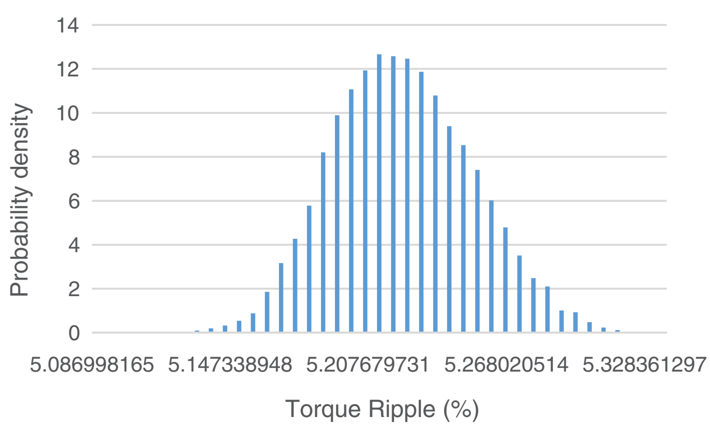

Figure 1.47 Torque ripple distribution on 10%-10%-1% design variable tolerances.

TABLE 1.16 10%-10%-1% tolerances on design variables

10% tolerance on P2 10% tolerance on P5 1% tolerance on P3	Mean value	Probability value
Running torque (Nm)	170.39	0.4667 (P > 170.58 Nm)
Ripple torque (%)	5.207	0.9315 (P < 5.2673%)

These plots show a significant reduction of scatter of both distributions. Table 1.16 presents the new mean value and probability results as numerical measurement to accept the statistical hypothesis for both running torque and torque ripple characteristics.

According to this analysis, almost 46.67% of all designs will have running torque values greater than 170.58 Nm. As far ripple torque characteristic is concerned the statistical test shows better level of significance. Almost 93.15% of all designs will have torque ripple values less than 5.2673%.

The scatter of outputs centralizes around mean of the population defining tighter tolerances for most sensitive parameters. Sensitivity analysis illustrated in Figure 1.48 shows further improvements if P5 (PM bridge) and P2 (slot opening) are considered with lower tolerance. The results of new Six Sigma analysis are presented in Table 1.17.

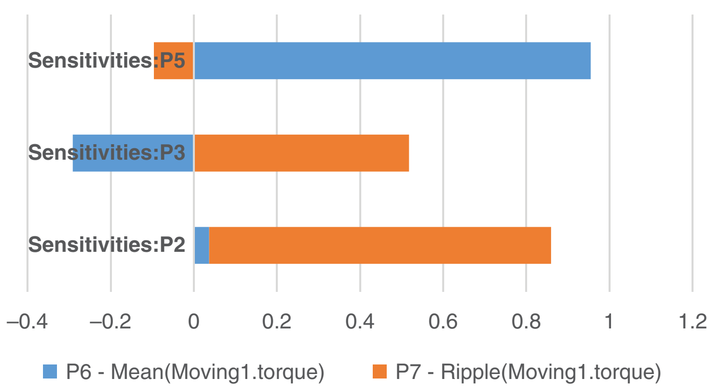

Figure 1.48 Sensitivity results for 10%-10%-1% design variable tolerances.

TABLE 1.17 5%-5%-1% tolerances on design variables

5% tolerance on P2 5% tolerance on P5 1% tolerance on P3	Mean value	Probability value
Running torque (Nm)	170.51	0.4411 (P > 170.58 Nm)
Ripple torque (%)	5.212	94.81 (P < 5.2673%)

TABLE 1.18 5%-1%-1% tolerances on design variables

5% tolerance on P2 1% tolerance on P5 1% tolerance on P3	Mean value	Probability value
Running torque (Nm)	170.54	0.3897 (P > 170.58 Nm)
Ripple torque (%)	5.22	0.9942 (P < 5.2673%)

Depending on targeted application, such analysis should always be a trade-off between the quality of the design and the cost of manufacturing to maintain low tolerance values. From last Six Sigma simulation (as reported in Table 1.18), tightening the tolerances on PM bridge dimension (P5) increases the probability of getting less torque ripples with a trade-off on getting higher running torque with respect to previous Six Sigma analysis.

REFERENCES

[1] D. M. Ionel and M. Rosu, “Short course: Introduction to electric machine design for manufacturing,” in *IEEE ITEC 2014*, Dearborn, MI, Jun. 2014.

[2] D. M. Ionel, S. J. Dellinger, R. J. Heideman, and A. E. Lesak, “Stator assembly for an electric machine and method of manufacturing the same,” U.S. Patent 7348706, Mar. 2008.

[3] D. M. Ionel, “High-efficiency variable-speed electric motor drive technologies for energy savings in the US residential sector,” in *Rec. IEEE Optim. 2010 Conf.*, Brasov, RO, May 2010, pp. 1403–1414.

[4] A. Fatemi, D. M. Ionel, N. A. O. Demerdash, S. Stretz, and T. M. Jahns, “RSM-DE-ANN sensitivity analysis of material cost in PM motors with distributed and concentrated windings,” in *Rec. IEEE ECCE 2016 Congress*, Milwaukee, WI, Sep. 2016, p. 7.

[5] M. Popescu, I. Foley, D. A. Staton, and J. E. Goss, “Multi-physics analysis of a high torque density motor for electric racing cars,” in *Rec. IEEE ECCE 2015 Congress*, Montreal, QC, Sep. 2016, p. 8.

[6] A. Fatemi, D. M. Ionel, M. Popescu, and N. A. O. Demerdash, “Design optimization of spoke-type PM motors for formula E racing cars,” in *Rec. IEEE ECCE 2016 Congress*, Milwaukee, WI, Sep. 2016, p. 8.

[7] J. Pyrhonen, T. Jokinen, and V. Hrabovcova, Design of Rotating Electrical Machines. John Wiley & Sons, 2010.

[8] J. Hendershot and T. J. E Miller, Design of Brushless Permanent Magnet Machines. Motor Design Books LLC, 2010.

[9] J.-S. Hwang, K.-H. Kim, Y.-T. Kim, and S.-M. Baek, “Parameter optimization of field oriented control with 6 sigma tool,” *IEEE ISIE*, vol. 3, pp. 1866–1870, Jun. 2001.

[10] G. Ombach and J. Junak, “Design of PM brushless motor taking into account tolerances of mass production - six sigma design method,” *IAS Annual Meeting*, vol. 49, no. 7, pp. 2139–2146, Sep. 2007.

[11] X. Meng, S. Wang, J. Qiu, Q. Zhang, J. G. Zhu, Y. Guo, and D. Liu,“Robust multilevel optimization of PMSM using design for six sigma,” *IEEE Trans. Magn.*, vol. 47, no. 10, pp. 3248–3251, Oct. 2011.

[12] G. Lei, Y. G. Guo, J. G. Zhu, T. S. Wang, X. M. Chen, and K. R. Shao, “System level six sigma robust optimization of a drive system with PM transverse flux machine,” *IEEE Trans. Magn.*, vol. 48, no. 2, pp. 923–926, Feb. 2012.

[13] G. Lei, J. G. Zhu, Y. G. Guo, J. F. Hu, W. Xu, and K. R. Shao, “Robust design optimization of PM-SMC motors for six sigma quality manufacturing,” *IEEE Trans. Magn.*, vol. 49, no. 7, pp. 3953–3956, Jul. 2013.

[14] G. Lei, J. Zhu, Y. Guo, K. Shao, and W. Xu, “Multiobjective sequential design optimization of PM-SMC motors for six sigma quality manufacturing,” *IEEE Trans. Magn.*, vol. 50, no. 2, Feb. 2014.

[15] G. Lei, J. G. Zhu, Y. G. Guo, J. F. Hu, W. Xu, and K. R. Shao, “Robust design optimization of PM-SMC motors for six sigma quality manufacturing,” *IEEE Trans. Magn.*, vol. 49, no. 7, pp. 3953–3956, Jul. 2013.

[16] G. Lei, T. Wang, J. Zhu, Y. Guo, and S. Wang, “System-level design optimization method for electrical drive systems—Robust approach,” *IEEE Trans. Ind. Electron.*, vol. 62, no. 8, pp. 4702–4713, Aug. 2015.

[17] Y.-K. Kim, J.-P. Hong, and J. Hur, “Torque characteristic analysis considering the manufacturing tolerance for electric machine by stochastic response surface method,” *IEEE Trans. Ind. Appl.*, vol. 39, no. 3, pp. 713–719, May/Jun. 2003.